1   **Title: Distinct phases of Polycomb silencing to hold epigenetic memory of cold in Arabidopsis**

2   **Authors:** Hongchun Yang[1]*, Scott Berry[1,2]*, Tjelvar S. G. Olsson[2], Matthew Hartley[2], Martin

3   Howard[2]†, Caroline Dean[1]†

4   **Affiliations:**

5   [1] Cell and Developmental Biology, John Innes Centre, Norwich Research Park, Norwich NR4 7UH,

6   UK.

7   [2] Computational and Systems Biology, John Innes Centre, Norwich Research Park, Norwich NR4

8   7UH, UK.

9   *Joint first authors

10   † Co-corresponding authors

11   **Abstract:**

12   **Gene silencing by Polycomb complexes is central to eukaryotic development. Cold-induced**

13   **epigenetic repression of *FLOWERING LOCUS C* (*FLC*) in the plant Arabidopsis provides an**

14   **opportunity to study initiation and maintenance of Polycomb silencing. Here, we show that a**

15   **subset of Polycomb Repressive Complex 2 factors nucleate silencing in a small region within**

16   ***FLC*, locally increasing H3K27me3 levels. This nucleation confers a silenced state that is**

17   **metastably inherited, with memory held in the local chromatin. Metastable memory is then**

18   **converted to stable epigenetic silencing through separate Polycomb factors, which spread across**

19   **the locus after cold to enlarge the domain containing H3K27me3. Polycomb silencing at *FLC***

20   **thus has mechanistically distinct phases, which involve specialization of distinct Polycomb**

21   **components to deliver first metastable, then long-term epigenetic silencing.**

22   **One Sentence Summary:** Specialisation of Polycomb complexes generates metastable, then long-

23   term memory, at an environmentally-regulated epigenetic target gene.

24

25   **Main Text:**

26   Chromatin-based epigenetic memory is all-or-nothing, with chromatin modifications propagating

27   bistable states of gene expression (*1-4*). One example is silencing of the floral repressor gene *FLC* in

28   response to prolonged cold (*5*), a process known as vernalization. This involves individual *FLC* loci

29   switching from an active to a stably repressed state in response to cold. This switching requires the

30   conserved Polycomb Repressive Complex 2 (PRC2) and occurs in two steps: first, nucleation of

31   H3K27me3 in a Polycomb Response Element (PRE)-like region of 2-3 nucleosomes close to the *FLC*

32 transcription start site during cold exposure, and second, spreading of H3K27me3 over the entire 7 kb

33 *FLC* locus when plants are returned to the warm. Full coverage with H3K27me3 is associated with

34 long-term epigenetic silencing and DNA methylation is not involved (6). Molecular and genetic

35 studies have identified much of the machinery required for *FLC* epigenetic silencing, but how

36 different factors interact dynamically in relation to the key events of nucleation and spreading has yet

37 to be determined.

38 The key molecular players involved in *FLC* epigenetic silencing are the PRC2 subunit

39 VERNALIZATION 2 (VRN2, a SU(Z)12 homolog), the plant-homeodomain proteins

40 VERNALIZATION INSENSITIVE 3 (VIN3) and VERNALIZATION 5 (VRN5), the H3K27me3

41 methyltransferases CURLY LEAF (CLF) and SWINGER (SWN) and the H3K27me3-binding protein

42 LIKE HETEROCHROMATIN PROTEIN 1 (LHP1) (*7-12*). To dissect the requirement for these

43 proteins during various stages of *FLC* silencing, we measured *FLC* expression in wild-type (Col-*FRI*)

44 and *vin3*, *vrn2*, *vrn5*, *lhp1,* and *clf* mutants (in a *FRI* background). *vin3*, *vrn2* and *vrn5* mutants all

45 showed impaired *FLC* shut-down during cold exposure and reactivation after cold (Fig. 1A and Fig.

46 S1) (*8-10*). In contrast, *FLC* repression in *lhp1* and *clf* mutants was unaffected at the end of cold

47 exposure but was unstable: repression was lost over 20 days after transfer to warm conditions (Fig. 1A

48 and Fig. S1). *VIN3* is upregulated during cold exposure (*9*), however its expression profile was

49 unchanged from wild-type in the other mutant backgrounds (Fig. S2A), indicating that altered *VIN3*

50 expression does not underlie the failure to stably silence *FLC*. The remaining factors *VRN2*, *VRN5*,

51 *SWN*, *CLF*, *LHP1* are not dynamically regulated during vernalization (Fig. S2B-D) (*10*).

52 Next, we measured H3K27me3 and H3K36me3 levels by chromatin immunoprecipitation (ChIP)

53 across the *FLC* locus in *vin3*, *vrn2*, *lhp1* and *clf* mutants. Wild-type plants show accumulation of

54 H3K27me3 and loss of H3K36me3 at the nucleation region during the cold (Fig. 1B,C and Fig. S3)

55 (*13,14*). H3K27me3 nucleation was disrupted in *vin3* and *vrn2* mutants. *lhp1* and *clf* mutants, on the

56 other hand, showed efficient nucleation – disagreeing with a reported role for LHP1 in nucleation

57 (*15*). Strikingly, *lhp1* and *clf* mutants failed to spread H3K27me3 at high levels across the *FLC* locus,

58 effectively decoupling nucleation and spreading. In these mutants, nucleation decayed slowly towards

59 pre-cold levels over the 20 days after cold. Concurrently, H3K36me3 levels and *FLC* expression

60 increased (Fig. 1 and Fig. S3), suggesting reversion of *FLC* loci from a nucleated and repressed state

61 to an active expression state.

62 We then compared *FLC* dynamics in double mutants *clf lhp1, clf vrn2* and *clf vin3,* with their

63 respective single mutants, which indicated that LHP1 and CLF function in the same genetic pathway

64 and that nucleation is upstream of spreading (Fig. 1A and Fig. S1). Thus, VIN3/VRN2/VRN5-

65 dependent H3K27me3-nucleation is required for *FLC* repression during the cold, and LHP1 and CLF

66 are required after cold to mediate spreading of H3K27me3 for long-term stable silencing. With little

67   or no spreading, H3K27me3 nucleation and silencing at *FLC* are maintained over approximately 20

68   days in *lhp1* and *clf*. Since plants are undergoing DNA replication, this suggests that the nucleated

69   state alone can maintain a metastable epigenetic memory of silencing at *FLC*.

70   Mathematical models based on local inheritance of modified histones and cis-acting positive

71   feedbacks had predicted that only the spread but not the nucleated state would be stable through DNA

72   replication (*2, 16*). We investigated the role of DNA replication by using the DNA synthesis inhibitor

73   roscovitine (*17*). In Arabidopsis, root meristem cells in our warm conditions replicate their DNA

74   approximately once per day (*18*). Roscovitine blocked cell division (Fig. S4A), but this had no effect

75   on *FLC* expression either before or after cold exposure in wild-type plants (Fig. S4B,C). In contrast,

76   *FLC* reactivation normally seen in *clf* and *lhp1* mutants was reduced (Fig. 2A and Fig. S4C) and

77   H3K27me3 nucleation was stable (Fig. 2B). Inhibition of DNA synthesis impaired spreading of

78   H3K27me3 in wild-type plants, even after 14 days of growth in the warm (Fig. 2B). These results

79   suggest that DNA replication/cell division is the major challenge to the stability of the nucleation peak

80   and that DNA replication/cell division is required for the H3K27me3 spreading.

81   To investigate this metastability at the single-cell level, we crossed the fluorescent *FLC-VENUS*

82   reporter (*1*) to *vin3*, *vrn2*, and *lhp1*. We then combined confocal microscopy and quantitative image

83   analysis (Fig. S5) to determine FLC-VENUS levels in root meristems. Before cold exposure, FLC-

84   VENUS is observed in all cells (Fig. S6A). After cold exposure and subsequent growth in the warm

85   for 7 days, wild-type plants showed long files of cells in either the ON or OFF expression states (Fig.

86   3A). These files demonstrate epigenetic maintenance of ON or OFF expression states as they are cell

87   lineages generated through anticlinal cell divisions from progenitors that experienced cold exposure

88   (*1*). In the nucleation mutants *vin3* and *vrn2*, FLC-VENUS remained ON in all cells. In the spreading

89   mutant *lhp1*, FLC-VENUS showed the wild-type ON/OFF distribution (Fig. 3A,B, and Fig. S6B,C).

90   Thus, nucleation is itself an all-or-nothing process (*14*), and *FLC* repression is maintained through

91   cell division in the *lhp1* mutant for at least 7 days after cold. To further test the stability of the

92   silenced state in *lhp1*, we exposed plants to an extended 10-week cold treatment. After 14 days of

93   subsequent growth in warm conditions, we observed the reappearance of a population of active cells

94   that did not occur in wild-type plants (Fig. 3C,D and Fig. S7). These *FLC*-ON cells often occurred as

95   isolated cells or as short files that likely represent clonal propagation of cells that stochastically

96   reactivate *FLC* expression. These data agree with population-level mRNA and ChIP measurements,

97   suggesting that the time-scales of reactivation observed at the population level in *lhp1* mutants

98   represent reactivation of *FLC*-expression at the single-cell level. These findings further support the

99   conclusion that LHP1 is not required for nucleation or for the propagation of metastable epigenetic

100   memory.

101   To explore whether this metastable epigenetic memory is stored in the local chromatin environment of

102   *FLC* (*1*), we generated *lhp1* plants carrying a single copy of *FLC-Venus* and *FLC-mCherry*. Before

103   cold FLC-Venus and FLC-mCherry were expressed in all root cells (Fig. S8A,B), whereas after cold

104   all four possible combinations of FLC-Venus/FLC-mCherry levels were found: ON/ON, ON/OFF,

105   OFF/ON, OFF/OFF (Fig. 3E and Figs. S8, S9). In both the wild-type and *lhp1* backgrounds, all

106   expression states occurred in files, indicating that the epigenetic state of the two *FLC* copies in the

107   same cell can be independently inherited. These data demonstrate that the metastable epigenetic

108   memory of *FLC* silencing is stored in cis at the *FLC* locus not only in the wild-type (*1*) but also in the

109   spreading mutant, *lhp1*.

110   Our previous models of vernalization-induced epigenetic silencing at *FLC* have been based on

111   inheritance of local histone modifications to daughter strands at DNA replication, followed by locally-

112   acting positive feedbacks to add similar modifications to newly incorporated histones (*2, 16*). Such

113   models require large chromatin regions to ensure that the chromatin state can be faithfully inherited

114   despite random partitioning of nucleosomes during DNA replication. Spreading of H3K27me3 to the

115   gene body (30-35 nucleosomes) fulfilled this requirement (*2*). While this mechanism can explain

116   long-term epigenetic memory at *FLC* in wild-type, difficulties arise in accounting for the metastable

117   silencing of *FLC* through DNA replication seen in *lhp1* and *clf* mutants, where H3K27me3 does not

118   accumulate to high levels outside the nucleation region. Assuming that memory is only held in a

119   nucleation region with 3 nucleosomes, the predicted dynamics would lead to a faster loss of silencing,

120   with almost one quarter of diploid cells reactivating at least one *FLC* copy after each DNA replication

121   (Supplemental Material). Such rapid dynamics predict 75% reactivation within a week and are

122   therefore inconsistent with the observed stability of *FLC* silencing in *lhp1* mutants (Fig. S10). These

123   conclusions are substantially unaffected even if we allow for a low level of H3K27me3 spreading, as

124   found in *lhp1* (Supplemental Material, Fig. S10C,D). We therefore propose that additional protein

125   factors present at the nucleation region may contribute directly in propagating metastable cis

126   epigenetic memory, potentially through self-reinforcing protein-protein interactions stabilising the

127   retention of factors such as VRN5.

128   To address this hypothesis, we mapped the binding of VIN3, VRN5, SWN, CLF and LHP1 (using

129   *VIN3-GFP/vin3*, *VRN5-YFP/vrn5*, *SWN-YFP*, *35S::GFP-CLF/clf* and *LHP1-eGFP/lhp1-6* (*10, 19-*

130   *21*)) at high spatial resolution across the *FLC* locus during vernalization. We verified that the newly

131   generated *VIN3-GFP* and *LHP1-eGFP* constructs complemented their respective mutant phenotypes

132   (Figs. S11 and S12), and that *VIN3-GFP* showed a similar dynamic expression pattern as endogenous

133   *VIN3* (Fig. S11). We also verified that VRN5, SWN, CLF and LHP1 tagged proteins localised to the

134   nuclei, and all the proteins including VIN3 could be efficiently enriched (Figs. S11C, S12F,G and

135   S13).

136 ChIP experiments indicated that VIN3, VRN5 and SWN were absent from the *FLC* locus before cold

137 (Fig. 4 and Fig. S14). During cold VIN3 protein was targeted to the *FLC* nucleation region (Fig. 4).

138 Similar to VIN3, localisation of SWN and VRN5 during cold was limited to the *FLC* nucleation

139 region. Together, these data indicate recruitment of VIN3/VRN5/SWN at the *FLC* nucleation region

140 during cold exposure. After cold, however, the dynamics of these three proteins differed: VIN3 was

141 lost within days, VRN5 was lost more slowly at the nucleation region over >10 days, but also

142 exhibited low level spreading over the gene body, while SWN occupancy increased when H3K27me3

143 spread to cover the *FLC* gene body. Levels of VIN3 at *FLC* correlated with the *VIN3* mRNA

144 expression level and also with bulk levels of VIN3-GFP protein (Fig. 4 and Fig. S11C). *VRN5*, *VRN2*,

145 *SWN*, *CLF* and *LHP1* were all more constitutively expressed (Fig. S2, B to E) (*10*). These findings

146 suggest that the cold-induced localization of VIN3 is essential to trigger nucleation and that dynamic

147 changes in the localization of the other proteins at *FLC* during vernalization are unlikely to be driven

148 by altered expression levels. The dynamics of VRN5 loss from the nucleation region after cold

149 parallels the loss of H3K27me3 at the nucleation region in *lhp1/clf* mutants (Fig. 1B,C, Fig.4 and Fig.

150 S15), suggesting that VRN5 defines the metastability of the nucleation-region memory.

151 To elaborate the mechanism underlying long-term epigenetic memory at *FLC* we examined the

152 dynamics of CLF and LHP1 in the different phases of vernalization. Both proteins showed similar

153 levels at *FLC* during and after cold exposure: both were associated with *FLC* chromatin before cold;

154 showed limited increases during cold; and, similar to SWN, increased in occupancy at the nucleation

155 region after cold (Fig. 4). LHP1 and CLF also showed more pronounced spreading to the gene body

156 after cold than SWN (Fig. 4), a feature which is consistent with their mutant phenotypes showing

157 reduced H3K27me3 domain size at *FLC* and genome-wide (*22, 23*). LHP1 and CLF physically

158 interact through additional PRC2 components (*24*), and furthermore both LHP1 and other PRC2-

159 subunits bind H3K27me3 (*25-27*), so our observed co-localisation of CLF and H3K27me3 suggests

160 that CLF likely deposits H3K27me3 in the *FLC* gene body. These reading and writing functions of

161 PRC2 and LHP1 for H3K27me3 may contribute to reinforcing the repressive chromatin state in the

162 *FLC* gene body, consistent with its long-term stability.

163 Our analysis of cold-induced epigenetic silencing at *FLC* clarifies the sequence of events involved in

164 Polycomb silencing of a genomic locus. Specialized Polycomb components function in two phases of

165 cis-inherited silencing that are genetically and mechanistically separate, to confer first reversible and

166 then long-term epigenetic memory (Fig. S16).

167

168 **References and Notes**

169 1.   S. Berry, M. Hartley, T. S G. Olsson, C. Dean, M. Howard, Local chromatin environment of a
170   Polycomb target gene instructs its own epigenetic inheritance. *Elife* **4**, (2015).

171 2.   A. Angel, J. Song, C. Dean, M. Howard, A Polycomb-based switch underlying quantitative
172   epigenetic memory. *Nature* **476**, 105-108 (2011).

173 3.   L. Bintu *et al.*, Dynamics of epigenetic regulation at the single-cell level. *Science* **351**, 720-
174   724 (2016).

175 4.   M. J. Obersriebnig, E. M. Pallesen, K. Sneppen, A. Trusina, G. Thon, Nucleation and
176   spreading of a heterochromatic domain in fission yeast. *Nat Commun* **7**, 11518 (2016).

177 5.   S. D. Michaels, R. M. Amasino, *FLOWERING LOCUS C* encodes a novel MADS domain
178   protein that acts as a repressor of flowering. *Plant Cell* **11**, 949-956 (1999).

179 6.   E. Jean Finnegan *et al.*, The downregulation of *FLOWERING LOCUS C* (*FLC*) expression in
180   plants with low levels of DNA methylation and by vernalization occurs by distinct
181   mechanisms. *Plant J* **44**, 420-432 (2005)

182 7.   F. De Lucia, P. Crevillen, A. M. Jones, T. Greb, C. Dean, A PHD-polycomb repressive
183   complex 2 triggers the epigenetic silencing of *FLC* during vernalization. *Proc Natl Acad Sci*
184   *U S A* **105**, 16831-16836 (2008).

185 8.   A. R. Gendall, Y. Y. Levy, A. Wilson, C. Dean, The *VERNALIZATION 2* gene mediates the
186   epigenetic regulation of vernalization in *Arabidopsis*. *Cell* **107**, 525-535 (2001).

187 9.   S. Sung, R. M. Amasino, Vernalization in *Arabidopsis thaliana* is mediated by the PHD
188   finger protein VIN3. *Nature* **427**, 159-164 (2004).

189 10.   T. Greb *et al.*, The PHD finger protein VRN5 functions in the epigenetic silencing of
190   *Arabidopsis FLC*. *Curr Biol* **17**, 73-78 (2007).

191 11.   J. S. Mylne *et al.*, LHP1, the *Arabidopsis* homologue of HETEROCHROMATIN
192   PROTEIN1, is required for epigenetic silencing of *FLC*. *Proc Natl Acad Sci U S A* **103**, 5012-
193   5017 (2006).

194 12.   S. Sung *et al.*, Epigenetic maintenance of the vernalized state in *Arabidopsis thaliana* requires
195   LIKE HETEROCHROMATIN PROTEIN 1. *Nat Genet* **38**, 706-710 (2006).

196 13.   H. Yang, M. Howard, C. Dean, Antagonistic Roles for H3K36me3 and H3K27me3 in the
197   Cold-Induced Epigenetic Switch at *Arabidopsis FLC*. *Curr Biol* **24**, 1793-1797 (2014).

198   14.   A. Angel *et al.*, Vernalizing cold is registered digitally at *FLC*. *Proc Natl Acad Sci U S A* **112**,
199   4146-4151 (2015).

200   15.   W. Yuan *et al.*, A *cis* cold memory element and a *trans* epigenome reader mediate Polycomb
201   silencing of *FLC* by vernalization in *Arabidopsis*. *Nat Genet*, (2016).

202   16.   I. B. Dodd, M. A. Micheelsen, K. Sneppen, G. Thon, Theoretical analysis of epigenetic cell
203   memory by nucleosome modification. *Cell* **129**, 813-822 (2007).

204   17.   S. Planchais *et al.*, Roscovitine, a novel cyclin-dependent kinase inhibitor, characterizes
205   restriction point and G2/M transition in tobacco BY-2 cell suspension. *Plant J* **12**, 191-202
206   (1997).

207   18.   G. V. Reddy, M. G. Heisler, D. W. Ehrhardt, E. M. Meyerowitz, Real-time lineage analysis
208   reveals oriented cell divisions associated with morphogenesis at the shoot apex of
209   *Arabidopsis thaliana*. *Development* **131**, 4225-4237 (2004).

210   19.   J. I. Questa, J. Song, N. Geraldo, H. An, C. Dean, *Arabidopsis* transcriptional repressor VAL1
211   triggers Polycomb silencing at *FLC* during vernalization. *Science* **353**, 485-488 (2016).

212   20.   D. Schubert *et al.*, Silencing by plant Polycomb-group genes requires dispersed trimethylation
213   of histone H3 at lysine 27. *EMBO J* **25**, 4638-4649 (2006).

214   21.   D. Wang, M. D. Tyson, S. S. Jackson, R. Yadegari, Partially redundant functions of two SET-
215   domain polycomb-group proteins in controlling initiation of seed development in
216   *Arabidopsis*. *Proc Natl Acad Sci U S A* **103**, 13244-13249 (2006).

217   22.   H. Wang *et al.*, Arabidopsis Flower and Embryo Developmental Genes are Repressed in
218   Seedlings by Different Combinations of Polycomb Group Proteins in Association with
219   Distinct Sets of Cis-regulatory Elements. *PLoS Genet* **12**, e1005771 (2016).

220   23.   A. Veluchamy *et al.*, LHP1 Regulates H3K27me3 Spreading and Shapes the Three-
221   Dimensional Conformation of the Arabidopsis Genome. *PLoS ONE* **11**, e0158936 (2016).

222   24.   M. Derkacheva *et al.*, *Arabidopsis* MSI1 connects LHP1 to PRC2 complexes. *EMBO J* **32**,
223   2073-2085 (2013).

224   25.   C. Xu *et al.*, Binding of different histone marks differentially regulates the activity and
225   specificity of polycomb repressive complex 2 (PRC2). *Proc Natl Acad Sci U S A* **107**, 19266-
226   19271 (2010).

227 26.   K. H. Hansen *et al.*, A model for transmission of the H3K27me3 epigenetic mark. *Nat Cell*
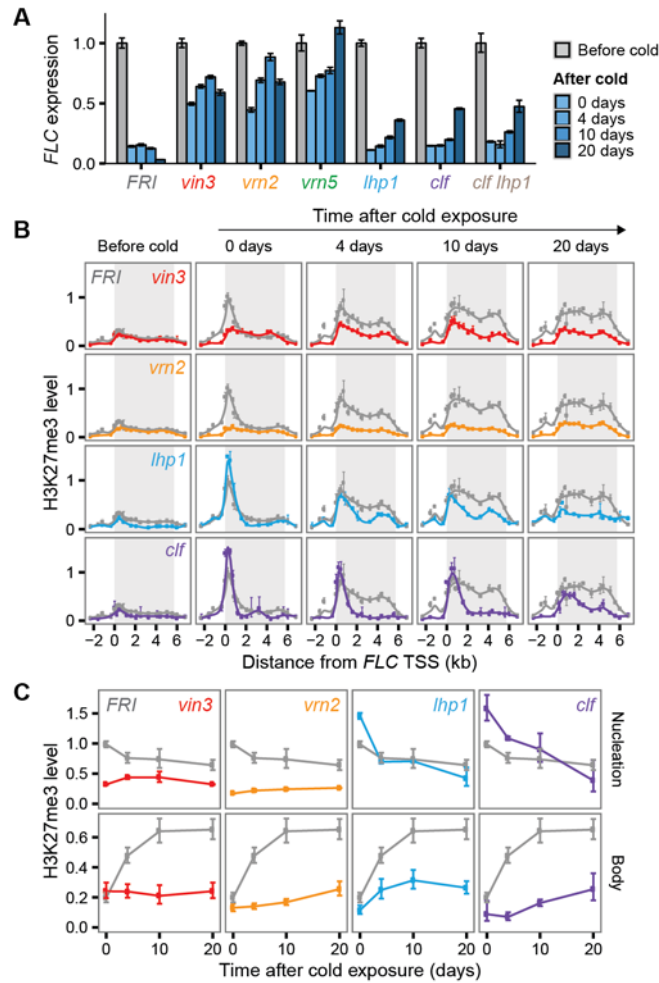228   *Biol* **10**, 1291-1300 (2008).

229 27.   X. Zhang *et al.*, The *Arabidopsis* LHP1 protein colocalizes with histone H3 Lys27
230   trimethylation. *Nat Struct Mol Biol* **14**, 869-871 (2007).

231

239

240

Figure 1: Nucleation and spreading are genetically separable. (**A**) *FLC* expression measured by RT-qPCR after a 6-week cold treatment. Data are represented relative to *UBC*, with different genotypes normalized to non-vernalized *FLC* levels. Error bars represent s.e.m (n ≥ 3). (**B**) H3K27me3 ChIP across the *FLC* locus before cold and after a 6-week cold treatment. Data expressed relative to *STM*. Error bars represent s.e.m. (n ≥ 3). Curves fitted using LOESS local regression (Supplementary Materials). (**C**) H3K27me3 ChIP data averaged over 2 primers in the *FLC* nucleation region and 5 primers in the gene body (Table S1). Error bars represent s.d.

248

249
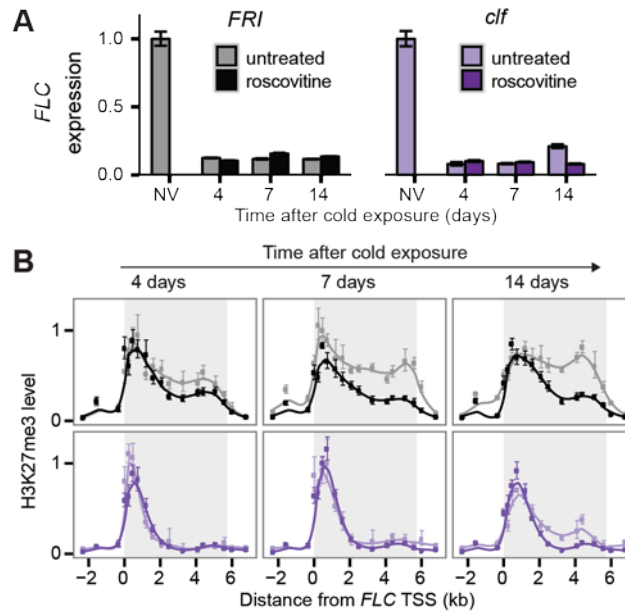
Figure 2: Nucleation is maintained but spreading is inhibited by roscovitine treatment. (**A**) *FLC* expression after 6-weeks cold in wild-type (*FRI*) or a *clf* mutant, with or without subsequent roscovitine treatment in warm conditions. Data are represented relative to *UBC*, with each genotype normalized to its respective non-vernalized (NV) *FLC* level. Error bars represent s.e.m (n = 4). (**B**) H3K27me3 levels at *FLC* after 6-weeks cold with or without subsequent roscovitine treatment in warm conditions. Data expressed relative to *STM*. Error bars represent s.e.m. (n ≥ 3). Dark shades (black and purple) represent roscovitine treatment, while light shades (grey and light purple) represent untreated samples. Curves fitted using LOESS local regression (Supplementary Materials).

258

259

260
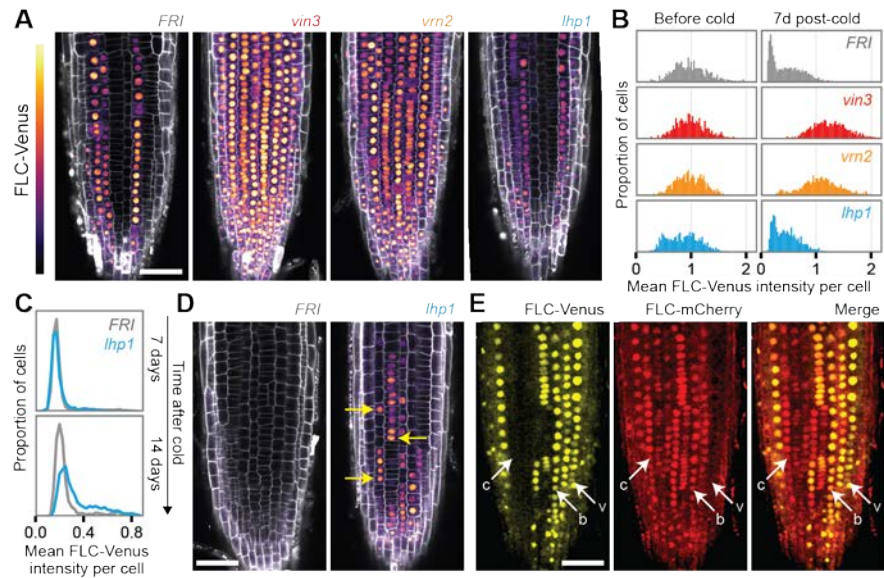
Figure 3: 'Metastable' cis epigenetic memory of *FLC* expression. (A) FLC-Venus intensity in root meristems in the wild-type and the various mutant backgrounds indicated. Plants were imaged 7 days after a 7-week cold treatment. **(B)** Histograms of single-cell FLC-Venus intensities obtained from automated image quantification, before cold and 7 days after a 7-week cold treatment. Number of roots and cells analysed for each treatment listed in Table S2. **(C)** Distribution of single-cell FLC-Venus intensities in *FRI* and *lhp1*, 7- and 14-days after a 10-week cold treatment. Number of roots and cells analysed for each treatment listed in Table S2. **(D)** FLC-Venus imaged 14 days after a 10-week cold treatment in the wild-type and *lhp1* mutant. Arrows in *lhp1* plants indicate cells that show discontinuous expression relative to a neighbouring cell of the same file. **(E)** FLC-Venus and FLC-mCherry intensities in root meristems 10 days after a 6-week cold treatment in the *lhp1* mutant. The following notation is used to indicate files of cells in the various expression states: Both expressed, b; FLC-Venus only, v; FLC-mCherry only, c. Scales bars in (A), (D) and (E) are 50μm.

273

274
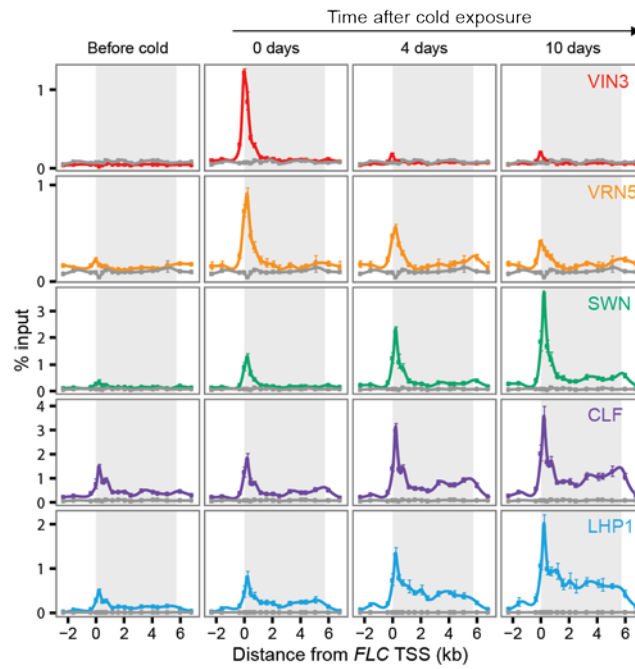
Figure 4: Dynamics of protein occupancy during vernalization. ChIP for indicated tagged proteins across the *FLC* locus before cold and after a 6-week cold treatment. The non-transgenic plant *FRI* was used as background control (grey line). Error bars represent s.e.m. (n = 3). Curves fitted using LOESS local regression (Supplementary Materials).

1

2

3

4 # Supplementary Materials for

5

6 **Distinct phases of Polycomb silencing to hold epigenetic memory of cold in Arabidopsis**

7

8 Hongchun Yang[1]*, Scott Berry[1,2]*, Tjelvar S. G. Olsson[2], Matthew Hartley[2], Martin Howard[2]†,
9 Caroline Dean[1]†

10 correspondence to: Martin.Howard@jic.ac.uk and caroline.dean@jic.ac.uk

11

12

13 **This PDF file includes:**

14

15 Materials and Methods

16 References (*28-47*)

17 Figs. S1 to S16

18 Tables S1 to S2

19

20 **Materials and Methods**

21 <u>Plant material and transgenic constructs</u>

22 All mutants and transgenic lines were in the FRI^{sf2} background, which was described previously (*28*).

23 Mutant alleles were also as described previously, *vin3* (*vin3-4*, (*29*)), *vrn5* (*vrn5-8*, (*10*)), *clf* (*clf-81*,

24 (*30*)), *lhp1* (*lhp1-3*, (*31*), *lhp1-6*, SALK_011762 (*32*)). When not specified, *lhp1* refers to *lhp1-3*. Col

25 *vrn2-1* was obtained by crossing Ler *vrn2-1* (*8*) to FRI^{sf2} Col-0 five times, selecting for the *vrn2-1*

26 mutant allele. Double mutants were generated by crosses between homozygous mutants and were

27 selected by PCR-based genotyping.

28

29 Previously generated *FLC-Venus / FRI^{sf2} flc-2* or *FLC-mCherry / FRI^{sf2} flc-2* lines (*1*) were crossed

30 into several of these mutant backgrounds. Using TAIL-PCR (*33*), the insertion sites for these *FLC-*

31 *Venus* and *FLC-mCherry* transgenes were mapped to chromosome 4 (within At4g12020, and

32 upstream of At4g05018, respectively). This allowed PCR-based identification of plants that were

33 homozygous for these transgenes. Plants containing a single copy of *FLC-Venus* and *FLC-mCherry* in

34 either *FRI^{sf2} flc-2* or *FRI^{sf2} lhp1-3* were selected from segregating F2 populations by PCR genotyping.

35 Genotyping primers are listed in Table S1.

36

37 *SWN-YFP* (*21*), and *35S::GFP-CLF/clf-28* (*20*) were both described previously. These lines were

38 crossed to the *FRI^{sf2}* background. The *VRN5-YFP* construct was described previously (*10*) and

39 transformed for this study into *vrn5-8*. *VIN3-GFP/vin3* was also described previously (*19*). The

40 *LHP1-eGFP* construct was generated for this study by gene synthesis (Invitrogen) and Golden Gate

41 cloning (*34*). The construct encodes *LHP1* genomic DNA from -2405 bp upstream of the ATG to

42 1134 bp downstream of the *LHP1* stop codon. *eGFP* is attached to the C-terminus via a Gly-Gly

43 linker. This construct was transferred to pSLJ755I6 (*35*) and transformed into *FRI^{sf2} lhp1-6*. Lines

44 were selected initially by complementation of the *lhp1* mutant phenotype and then by similarity of

45 expression level to endogenous *LHP1*.

46

47 <u>Growth conditions</u>

48 Seeds were surface sterilized and sown on MS-GLU (MS without glucose) media plates and kept at

49 4°C in the dark for 2 days. For non-vernalized (NV) conditions, seedlings were grown for 14 days in

50 long-day conditions (16 h light, 8 h darkness with constant 20°C). For vernalization treatment,

51 seedlings were pre-grown for 7 days in long-day conditions, and then moved to 5°C cold treatment in

52 short-day conditions (8 h light, 16 h darkness with constant 5°C) for a certain duration, such as 6

53 weeks (6W). For transfer experiments, after a certain duration of cold treatment, seedlings were

54 moved to long-day conditions on the plates (16 h light, 8 h darkness with constant 20°C) for another

55 specified duration, such as 10 days (T10). For the T20 transfer experiment, plants were transferred

56   after cold treatment from plates to soil, and were then grown in long-day conditions (16 h light 20°C,

57   8 h dark 18°C).

58

59   <u>Microscopy and image quantification</u>

60   Plants were grown vertically on MS plates with 1% (w/v) sucrose and 0.5% (w/v) Phytagel (Sigma-

61   Aldrich, P8169). FLC-Venus imaging was performed on a Leica SP8 X confocal microscope using a

62   20X/0.75NA objective lens, with illumination at 514 nm (Argon ion laser). Emissions from Venus

63   were detected between 518 nm and 555 nm using a cooled Leica HyD SMD detector in photon-

64   counting mode. Cell walls were visualized by adding propidium iodide (Sigma-Aldrich P4864) to the

65   immersion media at a concentration of 2 μg/mL. Propidium iodide was detected simultaneously with

66   FLC-Venus, by collecting emissions between wavelengths 610 nm and 680 nm. A z-step size of 0.95

67   μm was used for all confocal sections over a total depth of 20.9 μm from the upper surface (22 z-

68   slices per root). For the FLC-Venus FLC-mCherry double-label experiments, detection was sequential

69   (by z-plane) for the two fluorophores, using the 514 nm Argon ion laser for Venus and a White Light

70   Laser (Leica), tuned to 580 nm for mCherry. Venus was detected as described above, while mCherry

71   was detected between wavelengths 600 nm and 650 nm.

72

73   To generate Figs. 3 and S6-S9, z-stacks were processed in the following manner: images were first

74   aligned using the MultiStackReg plugin in Fiji (*36*). A Gaussian blur (Fiji, 0.2 μm filter size) was then

75   applied to all FLC-Venus images before performing a sum projection over 9 z-slices (8.55 μm). For

76   the cell wall stain, the central z-plane was extracted and overlaid on the FLC-Venus sum projection.

77   For Figs. 3E, S8, S9 (FLC-Venus/FLC-mCherry), similar steps were performed for both FLC-Venus

78   and FLC-mCherry, except a larger filter size of 0.6 μm was used for the Gaussian blur to reduce

79   noise.

80

81   <u>Quantitative image analysis</u>

82   Root images were analysed to generate mean FLC-Venus intensities per cell using a custom image

83   processing pipeline written in the Python programming language (*37*), using the jicbioimage (*38*),

84   Bio-Formats (*39*) and SimpleITK (*40*) libraries. Full source code for the pipeline is available at

85   https://github.com/JIC-Image-Analysis/root-3d-segmentation.

86

87   The pipeline consisted of four stages: generating three dimensional (3D) masks of the cell volume,

88   segmenting the area within the mask into individual cells, filtering the resulting segmentation and then

89   using this segmentation to compute mean FLC-Venus intensities per cell. A 3D root mask was

90   generated by first applying Otsu thresholding to the propidium iodide (cell wall) channel of the image.

91   A binary opening filter was applied to remove small objects from the thresholded image, and then the

92   convex hull of the result yielded the mask. Image segmentation was separately performed on the cell

93   wall channel. To preprocess the image, a median smoothing filter was applied (radius 1 voxel). The

94   gradient magnitude of the resultant image was calculated and a discrete Gaussian filter (radius 2

95   voxels) applied to the result. This image was then segmented with the morphological watershed

96   function provided by the SimpleITK library. SimpleITK's watershed algorithm provides an option to

97   dynamically filter the minima used as seeds to reduce over segmentation (*41*). The level for this

98   option was set to 0.644. The resulting segmentation was filtered by firstly removing any segmented

99   regions outside the mask and any touching the edges of the image. Then very small (<10000 voxels)

100   and large (>80000 voxels) segmented regions were removed.

101

102   The segmented cells were used to determine the mean FLC-Venus intensity by summing voxel

103   intensities from the FLC-Venus channel within a mask defined by the segmentation, and dividing by

104   the total cell volume in voxels. These per-cell mean intensities were used to generate histograms using

105   the R statistical computing environment (*42*).

106

107   <u>RNA expression analysis and qPCR</u>

108   RNA extraction was performed using the hot phenol method, as described elsewhere (*13*). Genomic

109   DNA contamination was removed by TURBO DNA-free (Invitrogen, AM1907) following the

110   manufacturer's guidelines, except that chloroform extraction and ethanol precipitation were used to

111   purify RNA after treatment. cDNA was synthesised by the SuperScript III First-strand synthesis

112   system (Invitrogen, 18080-051), using gene-specific primers or Oligo dT (12-18). cDNA was diluted

113   10 times before qPCR. All primers are listed in the Table S1. A standard reference gene *UBC* for gene

114   expression was used for normalization (*43*).

115

116   <u>Chromatin Immunoprecipitation (ChIP) and qPCR</u>

117   Histone modification ChIP was performed as previously described (*13*). The antibodies used were:

118   anti-H3 (Abcam, ab1791), anti-H3K27me3 (Millipore, 07-449) and anti-H3K36me3 (Abcam,

119   ab9050). All ChIP experiments were quantified by qPCR in triplicate with the indicated primer pairs

120   (Table S1). For H3K27me3 analysis, *SHOOT MERISTEMLESS* (*STM*), a standard reference gene for

121   H3K27me3, was used as the internal control and data are represented as the ratio of (H3K27me3

122   *FLC*/H3 *FLC*) to (H3K27me3 *STM*/H3 *STM*). In the case of H3K36me3, *ACTIN* (*ACT*) was used as

123   the internal control and the data are represented as H3K36me3 *FLC*/H3 *FLC*) to (H3K36me3 *ACT*/H3

124   *ACT*).

125

126   To measure protein levels at *FLC* during vernalization, protein ChIP experiments were performed as

127   described previously (*19*). In brief, purified nuclei were resuspended by RIPA buffer (1X PBS, 1%

128   IGEPAL CA-630 (Sigma, I8896), 0.5% sodium deoxycholate, 0.1% SDS, Roche Complete tablets

129   (Roche, 04693159001)), and then fragmented to ~500 bp by sonication (Agilent Bioruptor). After

130   sonication, the chromatin extract was cleared by centrifugation at 12,000 rpm for 10 minutes at 4°C.

131   Anti-GFP (Abcam, ab290) and Protein A Agarose/Salmon Sperm DNA (Millipore, 16-157) were used

132   in the ChIP pull-down. The enrichment levels of these proteins at *ACT*, *STM* and *AtSN1* were used as

133   controls. All primers used in the ChIP-qPCR experiments are listed in Table S1.

134

135   To plot the spatial profiles of protein and histone modification levels at *FLC*, curves were fitted to all

136   data points using local polynomial regression fitting, using the loess function in the R statistical

137   computing environment (*42*).

138

139   <u>Protein extraction, immunoprecipitation and immunoblotting</u>

140   Protein extraction, immunoprecipitation and immunoblots were performed as previously described

141   (*44*), with slight modifications. In brief, two-week-old seedlings were crosslinked in 1%

142   formaldehyde, ground in liquid nitrogen, and then suspended in RIPA buffer. Sonication was used to

143   release the chromatin. After clearing by centrifugation, the protein extract was incubated with anti-

144   GFP antibody (Abcam, ab290) for at least 2 hours, before adding Protein A beads to extract the

145   antibody-protein complexes. Beads were washed three times with RIPA buffer, and proteins were

146   eluted by boiling beads in Laemmli buffer. Proteins were separated on either 10% or 4-15% SDS-

147   PAGE gel (Bio-Rad 456-1085) and transferred to a nitrocellulose membrane (GE Healthcare Life

148   Sciences) for immunoblotting using an anti-GFP antibody (Roche, 11 814 460 001). Proteins were

149   detected by the SuperSignal West Femto Maximum Sensitivity Substrate (ThermoFisher Scientific).

150   To detect VIN3-GFP in the *VIN3-GFP/vin3* transgenic line, the protein was extracted using a

151   modified extraction buffer (100 mM Tris-HCl, pH 8.0, 150 mM NaCl, 2 mM EDTA, pH 8.0, 0.5%

152   IGEPAL CA-630, Roche cOmplete protease inhibitor). To allow quantitative comparisons between

153   different immunoprecipitations, it is necessary to ensure that the pulldown efficiency is constant. To

154   this end, protein extracted from 3 g of *VIN3-GFP/vin3* seedlings under each treatment was mixed with

155   protein extract from 0.25 g *FLC-Venus/FRI^sf flc-2* seedlings. 20 µl GFP-TrapM beads (Chromotek)

156   were added to the mixed protein extract. After 2 hours incubation at 4°C with gentle rotation, beads

157   were washed with extraction buffer, and proteins were eluted by boiling beads in Laemmli buffer.

158   Anti-tubulin (Sigma, T9026) was also used as a loading control.

159

160   <u>Roscovitine treatment</u>

161   To test the efficiency of roscovitine (Sigma, R7772) in blocking cell division and plant growth (*17*),

162   seedlings were grown vertically on GM-GLU plates for 12 days, and then transferred to fresh GM-

163   GLU plates containing 0, 2, 5, or 10 µM roscovitine respectively. Root tips of these seedlings were

164   aligned horizontally. 10 µM roscovitine efficiently blocked plant growth, and was therefore used in

165   subsequent RNA expression and ChIP experiments. Non-vernalized (14-day-old) seedlings or

166   seedlings exposed to cold for 6 weeks were transferred to liquid GM-GLU with 10 µM roscovitine in

167   long-day conditions with gentle shaking. After the specified duration of roscovitine treatment,

168   seedlings were harvested for either expression analysis or ChIP experiments.

169

170   <u>Stability of nucleation in histone-modification-based epigenetic memory</u>

171   Current models of histone-modification-based epigenetic memory require regions of chromatin of

172   several kilobases in size for stable memory propagation (*2, 16*). This requirement is due to the

173   segregation of nucleosomes that occurs between daughter DNA strands during DNA replication (*45*),

174   which results in each newly synthesized chromosome inheriting, on average, only half of the parental

175   histone modifications (*46*). In a previous model of chromatin-based *FLC* regulation (in wild-type

176   plants), epigenetic stability of the silenced state after cold was possible because H3K27me3 spread

177   rapidly to cover the whole locus (*2*). Loss of, on average, half of these histone modifications did not

178   result in loss of silencing because of the substantial number of remaining modifications which could

179   then feedback to fill in the missing marks. However, in *lhp1* and *clf*, we do not observe such high

180   levels of spreading, yet the nucleation peak with only a small number of H3K27me3 marks is still

181   maintained for many days after the cold – through many DNA replication events. This small size of

182   the H3K27me3-domain in the *FLC* nucleation region places strong theoretical constraints on the

183   ability of histone modifications in this region to be the sole heritable carriers of epigenetic memory.

184

185   We now derive an upper bound on the lifetime of the H3K27me3 nucleation peak after cold exposure

186   assuming that epigenetic memory is purely histone-modification based. In order to estimate the

187   maximum possible lifetime, our assumptions are conservative:

188   •   We assume that memory is stored solely in the nucleation region, consisting of three

189   nucleosomes.

190   •   Nucleosomes (more specifically H3/H4 tetramers) are randomly segregated between the two

191   daughter strands at DNA replication.

192   •   At the end of cold exposure, "nucleated" *FLC* contains three H3K27me3-covered nucleosomes,

193   and is perfectly stable outside of DNA replication.

194   •   Only one H3K27me3-modified nucleosome needs to be inherited by a daughter DNA strand to

195   propagate the "nucleated" state.

196   We will later slightly weaken the first and last of these assumptions to make our model more realistic.

197   With the above assumptions, the probability of a daughter DNA strand inheriting zero out of three

198   nucleosomes (and therefore losing silencing) is $1/2 \times 1/2 \times 1/2 = 1/8$. Since each cell contains two

199   homologous loci, the probability of losing silencing at one or more loci in a cell is

200 $$(1/8 \times 1/8) + 2(1/8 \times 7/8) = 15/64 \approx 0.23$$

201   Assuming a rate of cell division of once per day in the warm, this means that 23% of a population of

202   dividing cells will reactivate per day. Therefore, for a population of dividing cells, this gives the

203   following difference equation, with t in days,

$$P_{\text{silenced}}(t) \quad = \left(1 - \frac{15}{64}\right) P_{\text{silenced}}(t-1), \text{for } t \geq 1$$

$$= \left(\frac{49}{64}\right)^{t} P_{\text{silenced}}(0),$$

where P_{silenced} is the proportion of silenced cells.

Assuming that there is a lag of one day after cold before the onset of cell division and a further one day for the RNA produced from a reactivated *FLC* locus to be translated into visible protein in the cell, this can be re-formulated as,

$$P_{\text{FLC}}(t_{\text{after cold}}) = 1 - \left(\frac{49}{64}\right)^{t_{\text{after cold}}-2} P_{\text{silenced}}(0),$$

where $t_{\text{after cold}}$ is the number of days after cold exposure and P_{FLC} is the proportion of cells showing detectable FLC. With $P_{\text{silenced}}(0) = 1$, we find $P_{\text{FLC}}(7) \approx 74\%$ and $P_{\text{FLC}}(14) = 96\%$. However, it can be clearly seen from the microscopy images of FLC-Venus in the *lhp1* mutant at 7 and 14 days after 10 weeks of cold exposure (Figs. 3D, S7) that the actual proportion of cells in which FLC is visible is considerably lower, despite impaired spreading. In fact, we estimate that the proportion of cells with FLC intensity above background in *lhp1* is 6% and 30%, respectively for 7- and 14-days after a 10-week cold exposure (Fig. S10). Hence, with our above assumptions, a pure histone modification-based epigenetic memory is not consistent with the slow timescale of reactivation of *FLC* seen in the *lhp1* mutant.

One potential drawback of the above analysis is the assumption that H3K27me3 outside the nucleation region does not contribute to a histone-modification based memory. However, in *lhp1* a small amount of spreading is observed in the *FLC* gene body at 4 and 10 days after cold exposure. Accordingly, we now consider the case that any modified nucleosome at the locus can contribute, not just nucleosomes in the nucleation region. While it is difficult to estimate the number of modified nucleosomes from our ChIP-qPCR experiments, we again seek to make conservative estimates so that calculated lifetimes provide an upper bound. We calculate the maximum number of H3K27me3-modified nucleosomes at *FLC* in *lhp1* by first normalizing the LOESS smoothed ChIP profile to the maximum value observed at the nucleation region at the end of cold exposure. After subtracting the background calculated for H3K27me3 at the constitutively expressed *ACT* gene, we the integrate this ChIP profile from -1.5 to +5.5kb from the *FLC* transcription start site. Assuming a nucleosome spacing of 185 bp (*47*), this yields a total maximal number of H3K27me3 nucleosomes of 6.9 and 7.3 nucleosomes for 4 and 10 days after cold, respectively. That is, of the 35 additional nucleosomes considered outside the nucleation region, only four, on average, carry H3K27me3. Regardless of the molecular details of how these nucleosomes could contribute to maintaining H3K27me3 levels, we now repeat the above analysis in the case where more than 3 nucleosomes contribute equally to

epigenetic memory at the *FLC* locus. Generalising the above model to n nucleosomes gives a probability of losing silencing at one locus or the other in a cell of

$$\left(\frac{1}{2^n} \times \frac{1}{2^n}\right) + 2\left(\frac{1}{2^n} \times \left(1 - \frac{1}{2^n}\right)\right) = \frac{2^{n+1} - 1}{2^{2n}}.$$

Following the methodology above we find

$$P_{\text{FLC}}(t_{\text{after cold}}) = 1 - \left(1 - \frac{2^{n+1} - 1}{2^{2n}}\right)^{t_{\text{after cold}} - 2} P_{\text{silenced}}(0),$$

which for $n = 3$ reproduces our previous analysis. This more general formula is plotted for various values of n in Fig. S10C. For 7 nucleosomes this new model is now able to fit the data for *FLC* reactivation in the *lhp1* mutant. This model, however, relies on several unrealistic assumptions, such as a complete lack of replication-independent nucleosome exchange and the ability of inheritance of a single H3K27me3-modified nucleosome (out of ~38 in the 7 kb *FLC* locus) to direct silencing of the daughter DNA strand. If we relax this latter assumption, and require that at least two modified nucleosomes are required for inheritance of the repressed state, the probability of a daughter DNA strand inheriting zero or only one out of n nucleosomes (and therefore losing silencing) is $1/2^n + n/2^n = (n + 1)/2^n$. This formula then leads to a probability of reactivation per division of

$$\left(\frac{n + 1}{2^n} \times \frac{n + 1}{2^n}\right) + 2\left(\frac{n + 1}{2^n} \times \left(1 - \frac{n + 1}{2^n}\right)\right) = \frac{n + 1}{2^n}\left(2 - \frac{n + 1}{2^n}\right),$$

and a reactivated cell proportion of

$$P_{\text{FLC}}(t_{\text{after cold}}) = 1 - \left(1 - \frac{n + 1}{2^n}\left(2 - \frac{n + 1}{2^n}\right)\right)^{t_{\text{after cold}} - 2} P_{\text{silenced}}(0).$$

These reactivation dynamics are plotted alongside the experimental data for *lhp1* in Fig. S10D. As can be seen, the revised model reactivation is again much too quick in comparison with our experimental data. Overall, therefore, our experiments and analysis favour the hypothesis that histone modifications are not the only epigenetic memory storage elements.

References

28.   I. Lee, S. D. Michaels, A. S. Masshardt, R. M. Amasino, The late-flowering phenotype of *FRIGIDA* and mutations in *LUMINIDEPENDENS* is suppressed in the Landsberg *erecta* strain of *Arabidopsis*. *Plant J* **6**, 903-909 (1994).

262 29. D. M. Bond, I. W. Wilson, E. S. Dennis, B. J. Pogson, E. Jean Finnegan, *VERNALIZATION*
263   *INSENSITIVE 3* (*VIN3*) is required for the response of *Arabidopsis thaliana* seedlings
264   exposed to low oxygen conditions. *Plant J* **59**, 576-587 (2009).

265 30. G. T. Kim, H. Tsukaya, H. Uchimiya, The *CURLY LEAF* gene controls both division and
266   elongation of cells during the expansion of the leaf blade in *Arabidopsis thaliana*. *Planta* **206**,
267   175-183 (1998).

268 31. A. S. Larsson, K. Landberg, D. R. Meeks-Wagner, The *TERMINAL FLOWER2* (*TFL2*) gene
269   controls the reproductive transition and meristem identity in *Arabidopsis thaliana*. *Genetics*
270   **149**, 597-605 (1998).

271 32. J. M. Alonso *et al.*, Genome-wide insertional mutagenesis of *Arabidopsis thaliana*. *Science*
272   **301**, 653-657 (2003).

273 33. L. J. Qu, G. Qin, Generation and characterization of Arabidopsis T-DNA insertion mutants.
274   *Methods Mol Biol* **1062**, 241-258 (2014).

275 34. E. Weber, C. Engler, R. Gruetzner, S. Werner, S. Marillonnet, A modular cloning system for
276   standardized assembly of multigene constructs. *PLoS ONE* **6**, e16765 (2011).

277 35. J. D. Jones *et al.*, Effective vectors for transformation, expression of heterologous genes, and
278   assaying transposon excision in transgenic plants. *Transgenic Res* **1**, 285-297 (1992).

279 36. J. Schindelin *et al.*, Fiji: an open-source platform for biological-image analysis. *Nat Methods*
280   **9**, 676-682 (2012).

281 37.   Python Software Foundation. Python Language Reference, version 2.7.

282 38. T. S. Olsson, M. Hartley, jicbioimage: a tool for automated and reproducible bioimage
283   analysis. *PeerJ* **4**, e2674 (2016).

284 39. M. Linkert *et al.*, Metadata matters: access to image data in the real world. *J Cell Biol* **189**,
285   777-782 (2010).

286 40. B. C. Lowekamp, D. T. Chen, L. Ibanez, D. Blezek, The Design of SimpleITK. *Front*
287   *Neuroinform* **7**, 45 (2013).

288 41. R. Beare, G. Lehmann, The watershed transform in ITK - discussion and new developments.
289   *The Insight Journal* (2006)

290 42. R Development Core Team. 2016. R: a language and environment for statistical computing.
291   Vienna: R Foundation for Statistical Computing. https://www.R-project.org

292   43.   T. Czechowski, M. Stitt, T. Altmann, M. K. Udvardi, W. R. Scheible, Genome-wide
293   identification and testing of superior reference genes for transcript normalization in
294   Arabidopsis. *Plant Physiol* **139**, 5-17 (2005).

295   44.   H. Yang, M. Howard, C. Dean, Physical coupling of activation and derepression activities to
296   maintain an active transcriptional state at *FLC*. *Proc Natl Acad Sci U S A* **113**, 9369-9374
297   (2016).

298   45.   A. T. Annunziato, Split decision: what happens to nucleosomes during DNA replication? *J*
299   *Biol Chem* **280**, 12065-12068 (2005).

300   46.   C. Alabert *et al.*, Two distinct modes for propagation of histone PTMs across the cell cycle.
301   *Genes Dev* **29**, 585-590 (2015).

302   47.   T. Zhang, W. Zhang, J. Jiang, Genome-Wide Nucleosome Occupancy and Positioning and
303   Their Impact on Gene Expression and Evolution in Plants. *Plant Physiol* **168**, 1406-1416
304   (2015).

305

306
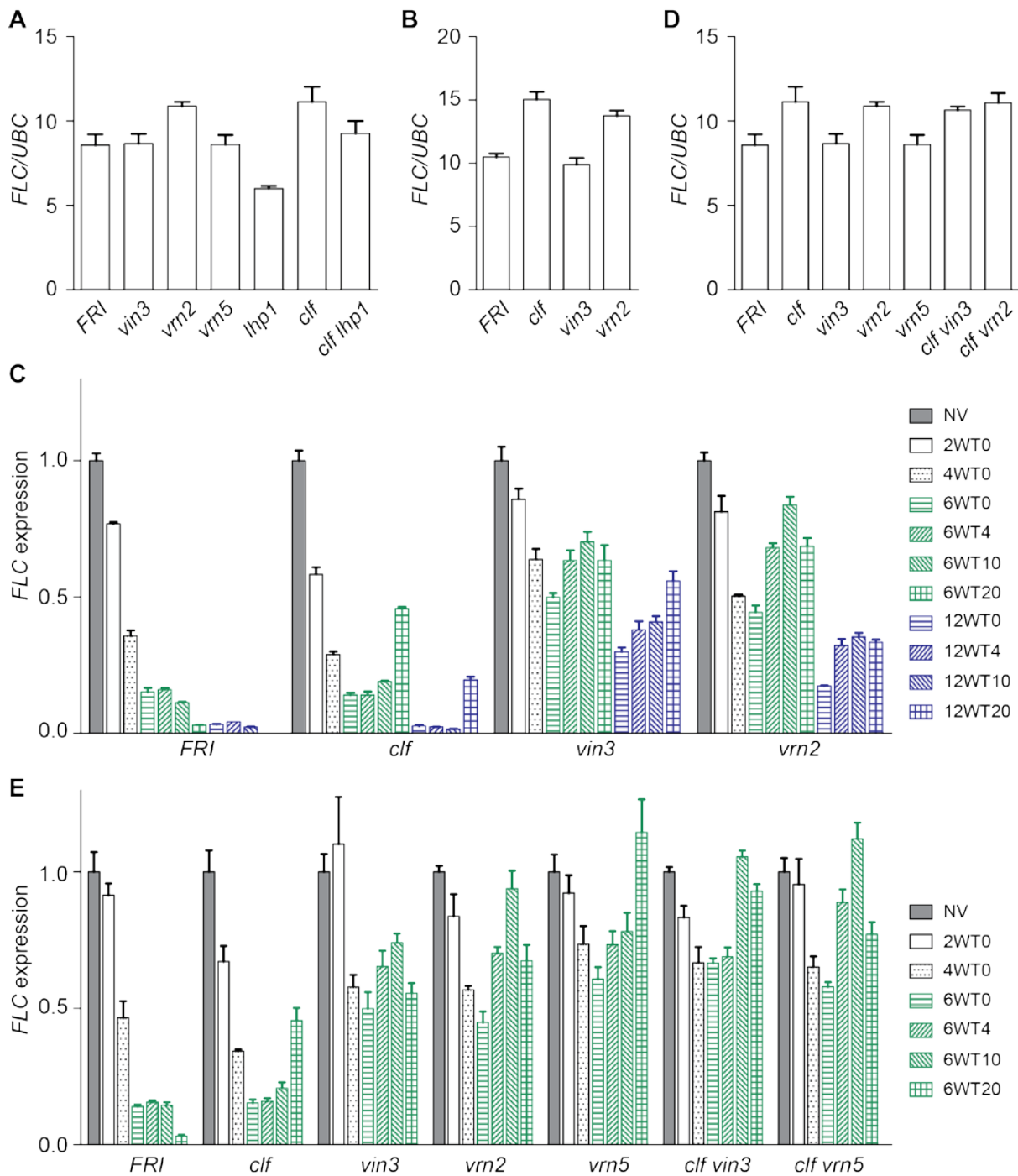
Fig. S1. *FLC* expression in mutant backgrounds. (**A**) *FLC* expression in mutants in non-vernalized conditions (from experiments in Fig.1A), measured by RT-qPCR. Data are represented relative to *UBC*. (**B**) *FLC* expression in *FRI*, *clf*, *vin3* and *vrn2* in non-vernalized conditions (from experiments in Fig. S1C), measured by RT-qPCR. Data are represented relative to *UBC*. (**C**) *FLC* expression in time course of cold treatment, measured by RT-qPCR. Data are represented relative to *UBC*, and then normalized to non-vernalized *FLC* levels. (**D**) *FLC* expression in non-vernalized conditions (from experiments in Fig. S1E). Data are represented relative to *UBC*. (**E**) *FLC* expression in time course of cold treatment, measured by RT-qPCR. Data are represented relative to *UBC*, and then normalized to

316   non-vernalized *FLC* levels. (C, E) NV, non-vernalized; #WT*, # weeks of cold treatment followed by

317   T * days of warm growth. All error bars represent s.e.m (n ≥ 3).

318
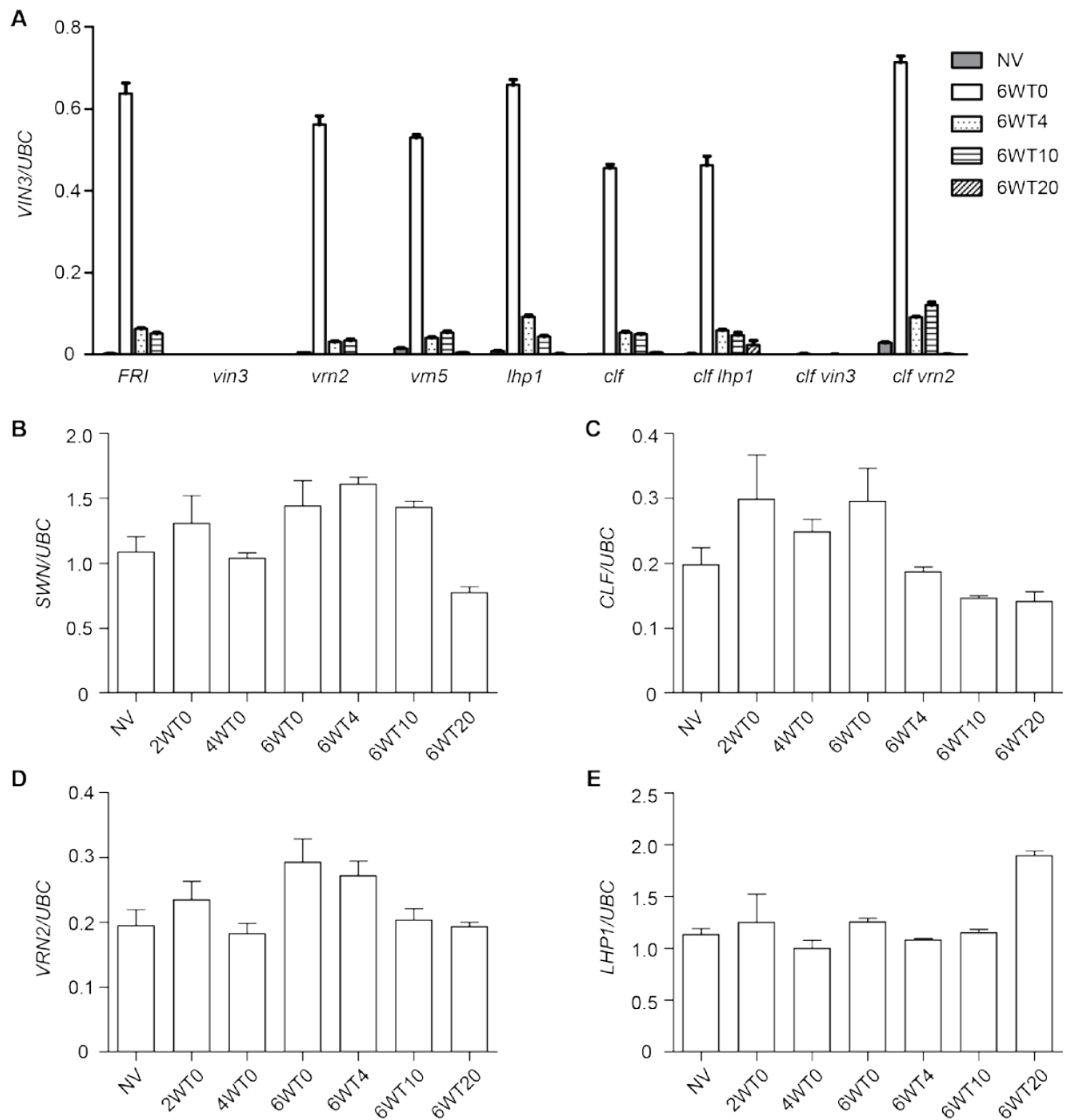
Fig. S2. Expression of Polycomb factors during vernalization. (**A**) *VIN3* expression measured
either in non-vernalized (NV) plants, or after a 6-week cold treatment (6W). Plants were transferred to
warm for 0, 4, 10 or 20 days (6WT0, 6WT4, 6WT10, 6WT20, respectively). Polycomb components
(**B**) *SWN*, (**C**) *CLF*, (**D**) *VRN2*, and (**E**) *LHP1* expression dynamics during vernalization measured by
RT-qPCR. Data are represented relative to *UBC*. Error bars represent s.e.m ($n \geq 3$).

324

325

326
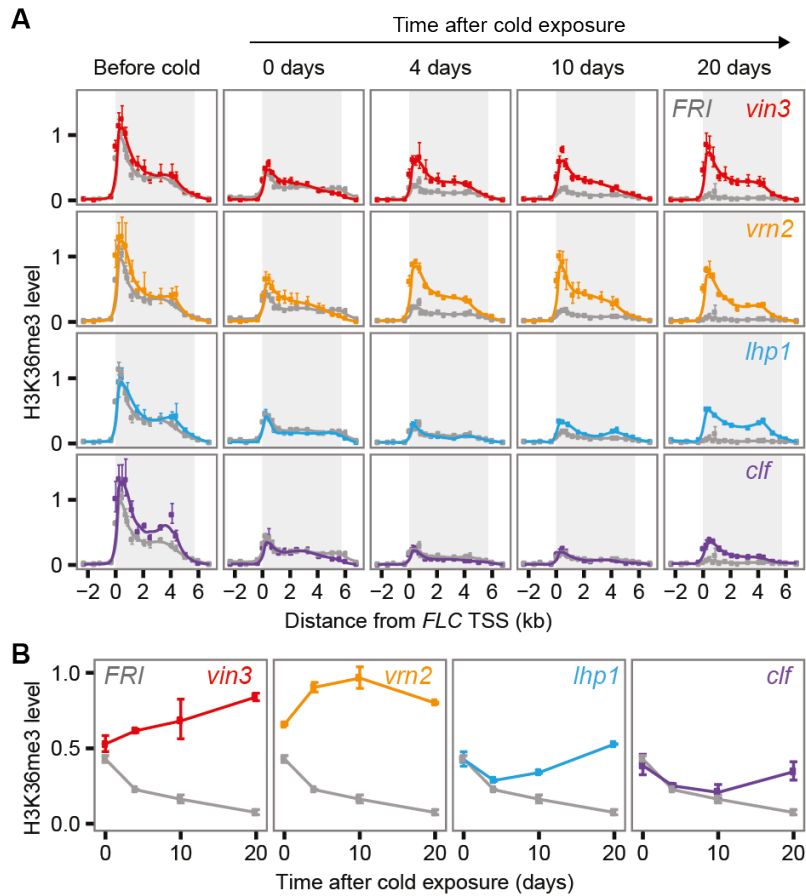
Fig. S3. H3K36me3 levels in the mutant backgrounds during vernalization. (A) H3K36me3 ChIP across the *FLC* locus before cold and after a 6-week cold treatment. Data normalised to H3 levels and then expressed relative to H3K36me3/H3 levels at *ACTIN*. Error bars represent s.e.m. (n ≥ 3). Curves fitted using LOESS local regression (Supplementary Materials). **(B)** H3K36me3 ChIP data averaged over 2 primers for the *FLC* nucleation region (Table S1). Error bars represent s.d.

332
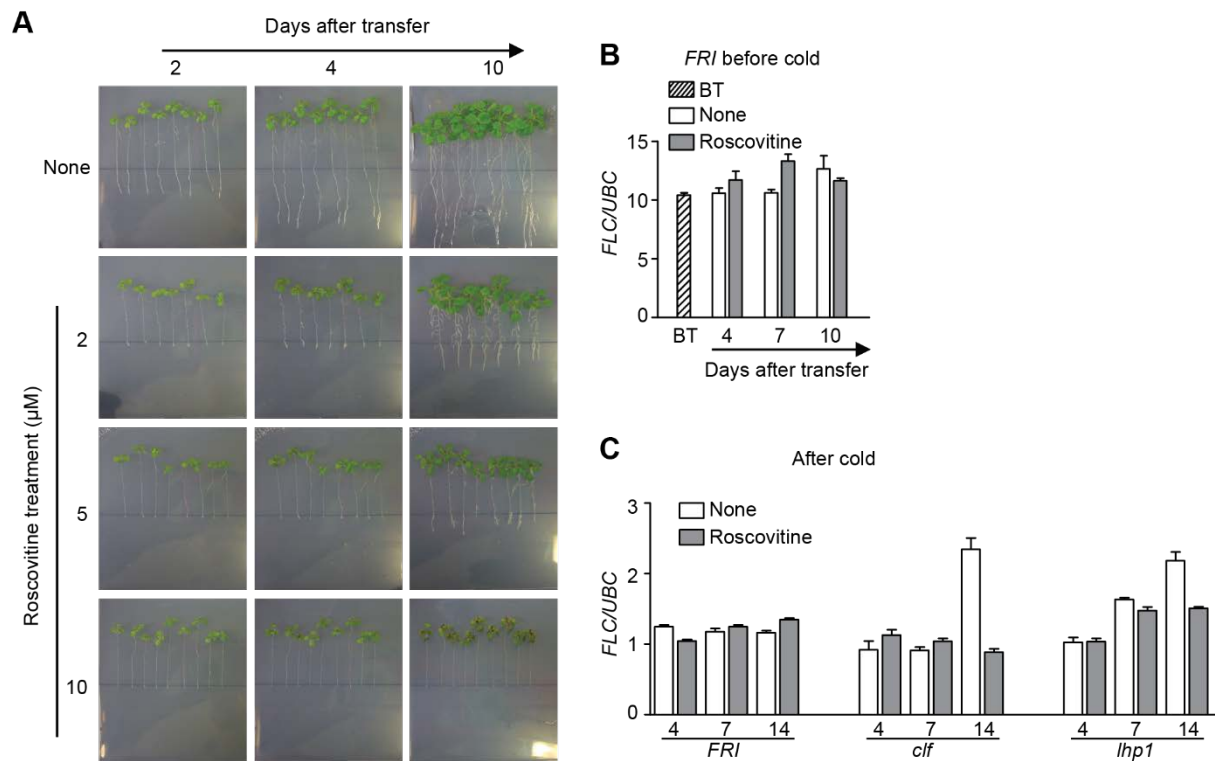
Fig. S4. *FLC* silencing is stably maintained after cold without DNA replication/cell division in wild-type and *clf*, *lhp1* mutants. (A) Roscovitine inhibits plant growth. Seedling were grown on GM-GLU vertical plates for 12 days, and then transferred to medium containing 0 or 2, 5, 10 µM roscovitine respectively. Root tips of these seedlings were aligned horizontally, as shown in the figure. (B) *FLC* expression during roscovitine treatment in non-vernalizing conditions. Wild-type 12-day old seedlings were treated with 0 or 10 µM roscovitine for 4, 7, and 10 days respectively. Untreated 12-day old seedlings were used as before treatment (BT) control. Data represented relative to *UBC*. Error bars represent s.e.m from 4 biological replicates. (C) *FLC* expression during roscovitine treatment after a 6-week cold exposure. Seedlings were transferred to warm conditions at the end of cold exposure and treated with 0 or 10 µM roscovitine for 4, 7, and 14 days. Data represented relative to *UBC*. Error bars represent s.e.m (n=4).

346
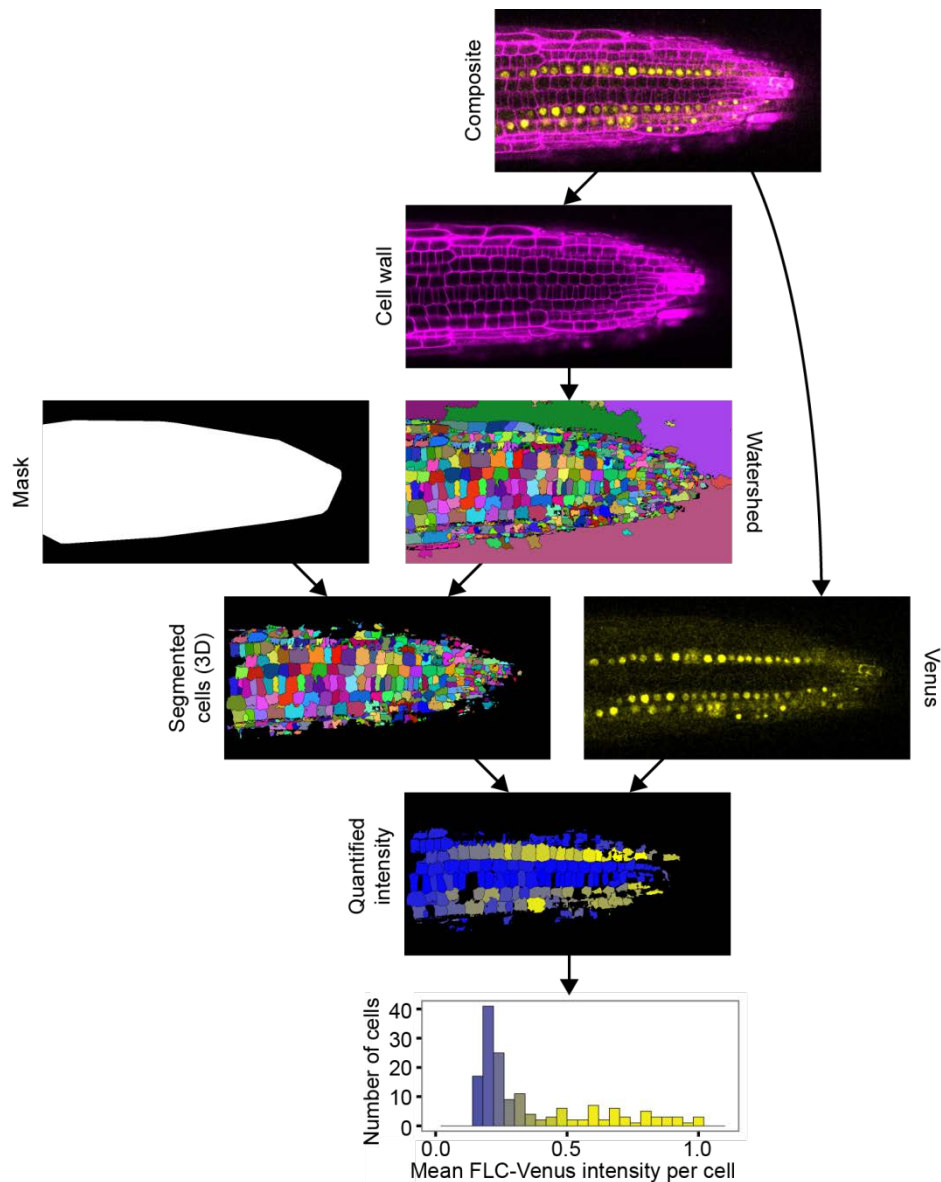
Fig. S5. Schematic of quantitative image analysis workflow for calculation of per-cell FLC-Venus fluorescence intensity. The propidium iodide staining channel representing the cell wall was used to generate both a mask of the root volume and a segmented image delineating individual regions (using the SimpleITK implementation of the Watershed segmentation algorithm). Root cells were identified as segmented regions within the mask. These cell regions were used to calculate the intensity of the FLC-Venus fluorescence channel on a per cell basis, giving the mean intensity per voxel for each cell. While all analysis was carried out in three dimensions, the images shown here represent a single plane of the confocal stack at different stages of the workflow.

355
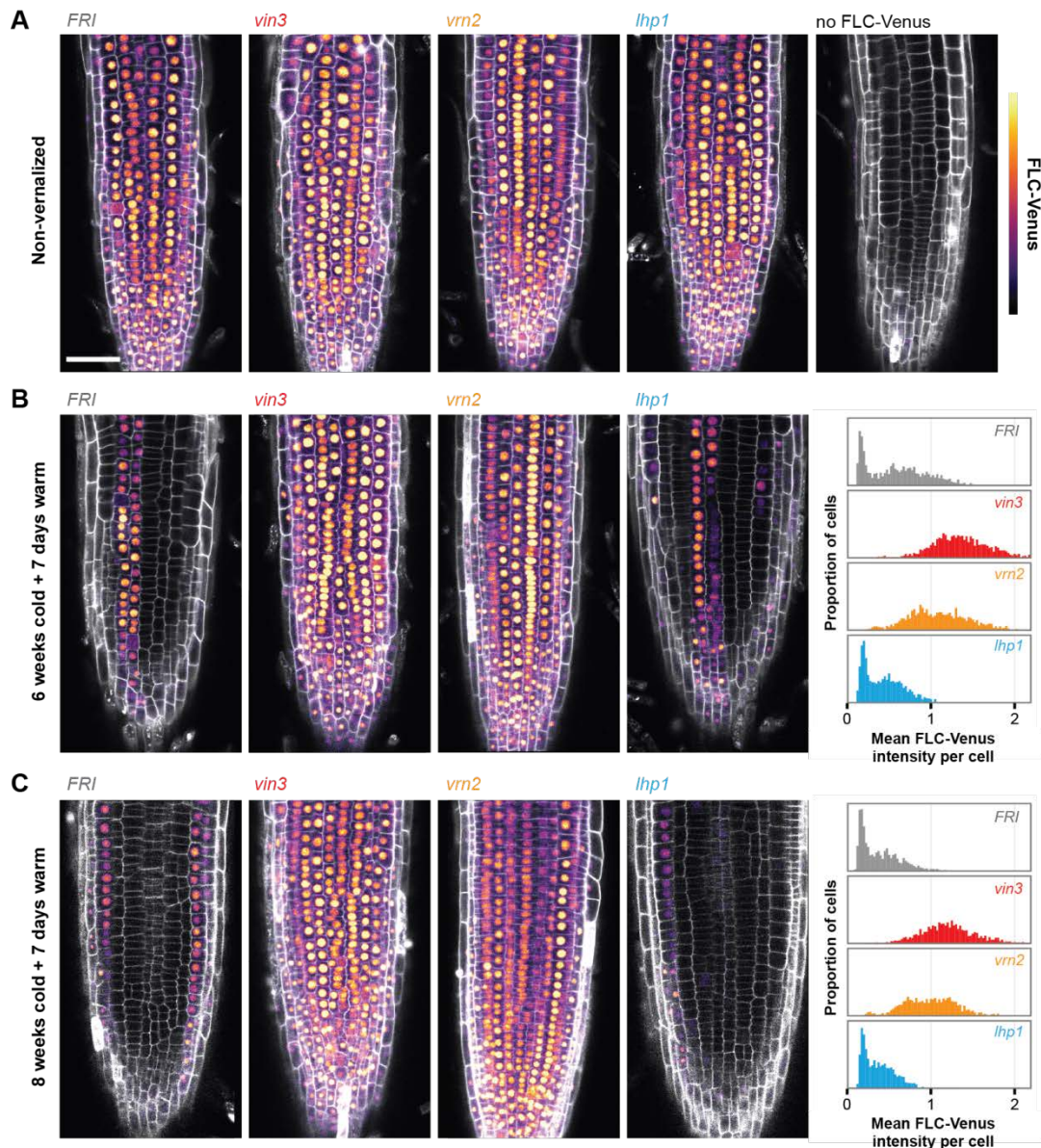
Fig. S6. Imaging FLC-Venus in root meristems. (**A**) FLC-Venus intensity in root meristems in wild-type and the various mutant backgrounds indicated in non-vernalized conditions. 14-day old plants were imaged. (**B**) and (**C**) FLC-Venus intensity and histograms of single-cell intensities obtained from automated image quantification, 7 days after a 6-week (B) or 8-week (C) cold treatment. Quantifications for non-vernalized roots are shown in Fig. 3B. Number of roots and cells analysed for each treatment listed in Table S2. The same image acquisition and processing settings were used for all roots. In composite images, FLC-Venus is a sum projection over 9 z-slices (8.55 μm), while the cell wall stain (propidium iodide) corresponds to a single central z-plane (Supplementary Materials). Scale bar in (A) represents 50 μm and is valid for all panels.

367
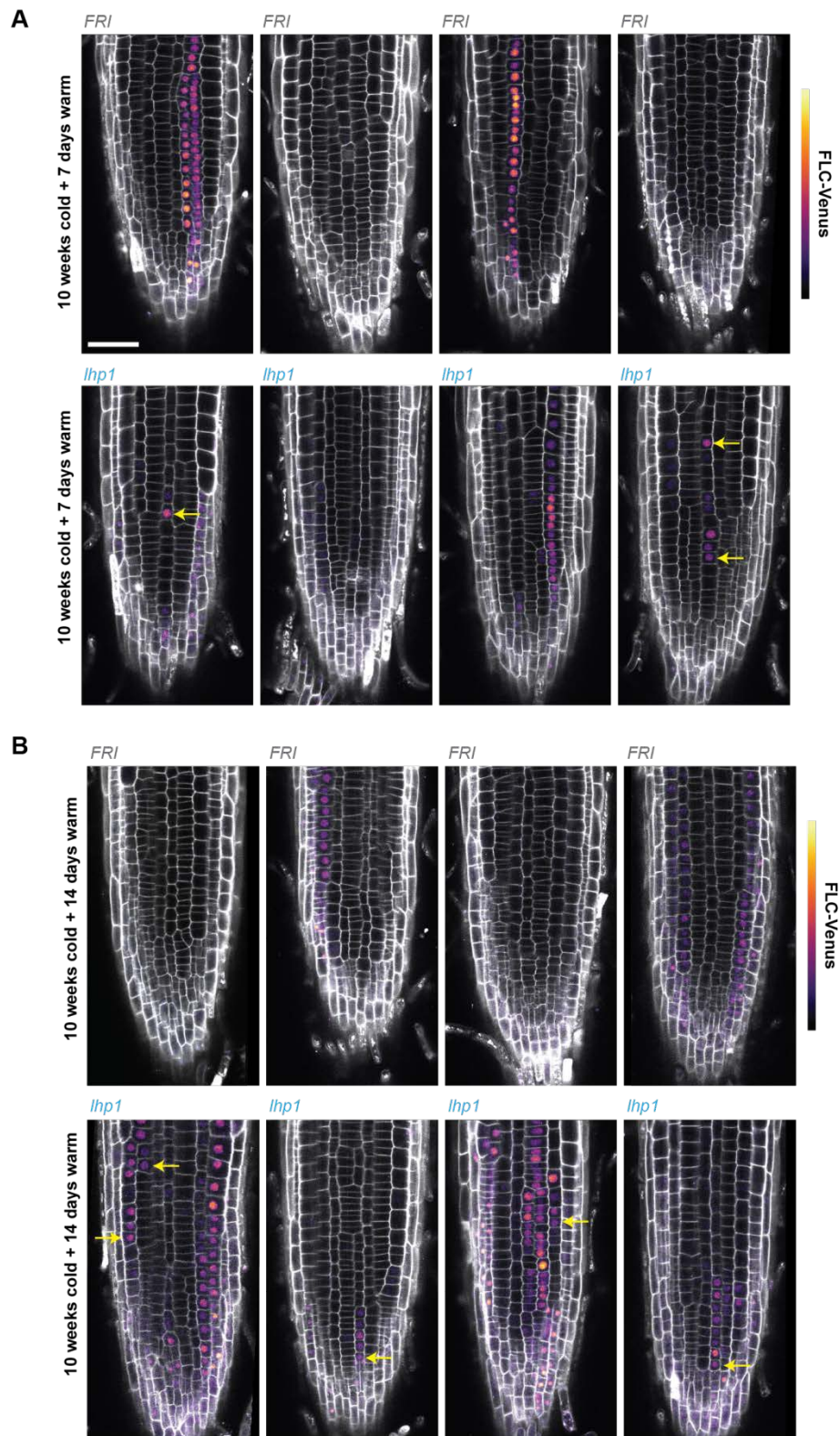
Fig. S7. Imaging FLC-Venus in root meristems after cold. (A,B) Examples of FLC-Venus in root
meristems of wild-type and *lhp1* plants either 7 days (A) or 14 days (B) after a 10-week cold-
treatment. The same image acquisition and processing settings were used for all roots. In composite
images, FLC-Venus is a sum projection over 9 z-slices (8.55 μm), while the cell wall stain (propidium
iodide) corresponds to a single central z-plane (Supplementary Materials). Arrows in *lhp1* plants

373   indicate cells that show discontinuous expression relative to a neighbouring cell of the same file.

374   Scale bar in (A) represents 50 μm and is valid for all panels.

375
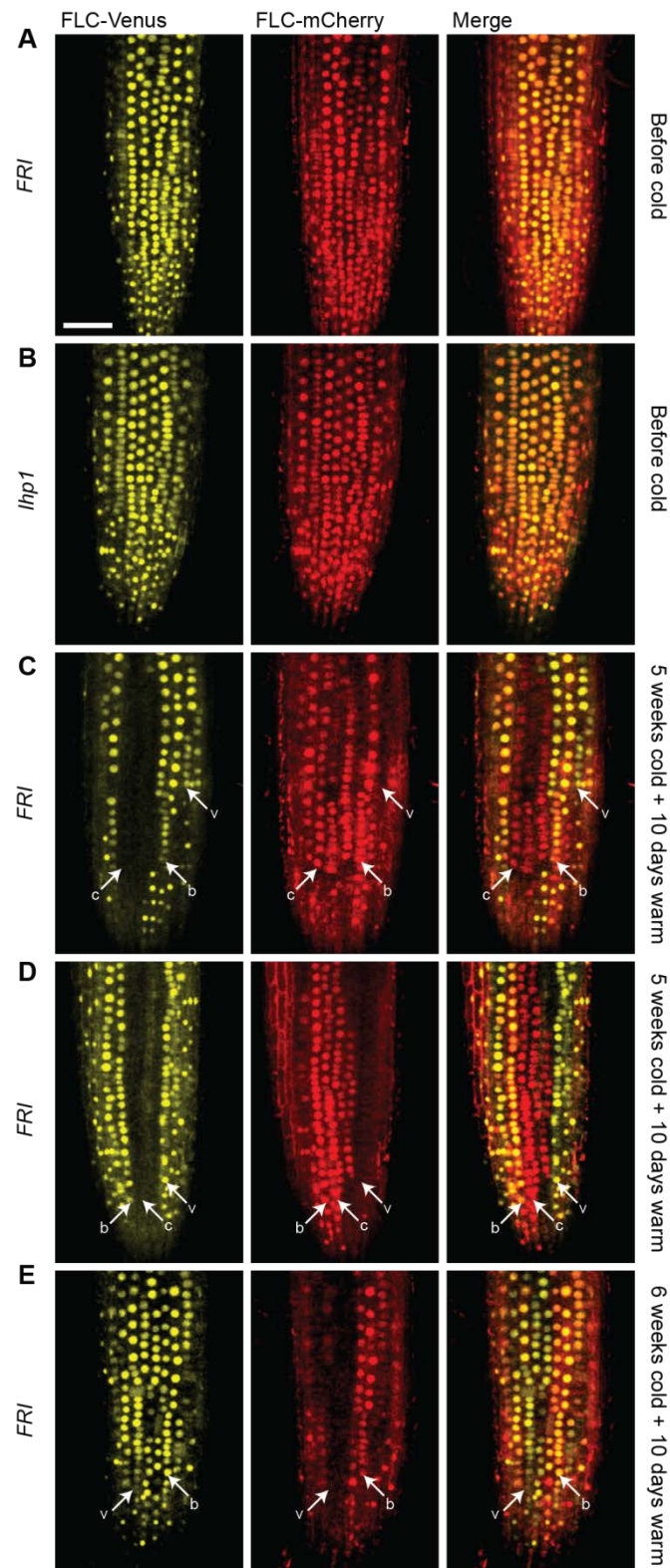
Fig. S8. Imaging FLC-Venus and FLC-mCherry in root meristems. (A,B) FLC-Venus and FLC-mCherry are uniformly present in all cells in non-vernalized plants for both wild-type (*FRI*) (A) and *lhp1* (B). **(C-E)** FLC-Venus / FLC-mCherry in wild-type roots after 5 weeks (C,D) or 6 weeks (E) cold exposure. Plants were grown for a further 10 days after cold before imaging. The following notation is used to label cell files in the various expression states: both expressed, b; FLC-Venus only,

382   v; FLC-mCherry only, c. All plants contain a single genomic copy of each of *FLC-Venus* and *FLC-*

383   *mCherry*. The same image acquisition and processing settings were used for all roots. Both channels

384   are sum projections over 9 z-slices (8.55 μm). Scale bar shown in upper left panel is 50 μm, and is

385   valid for all panels.

386
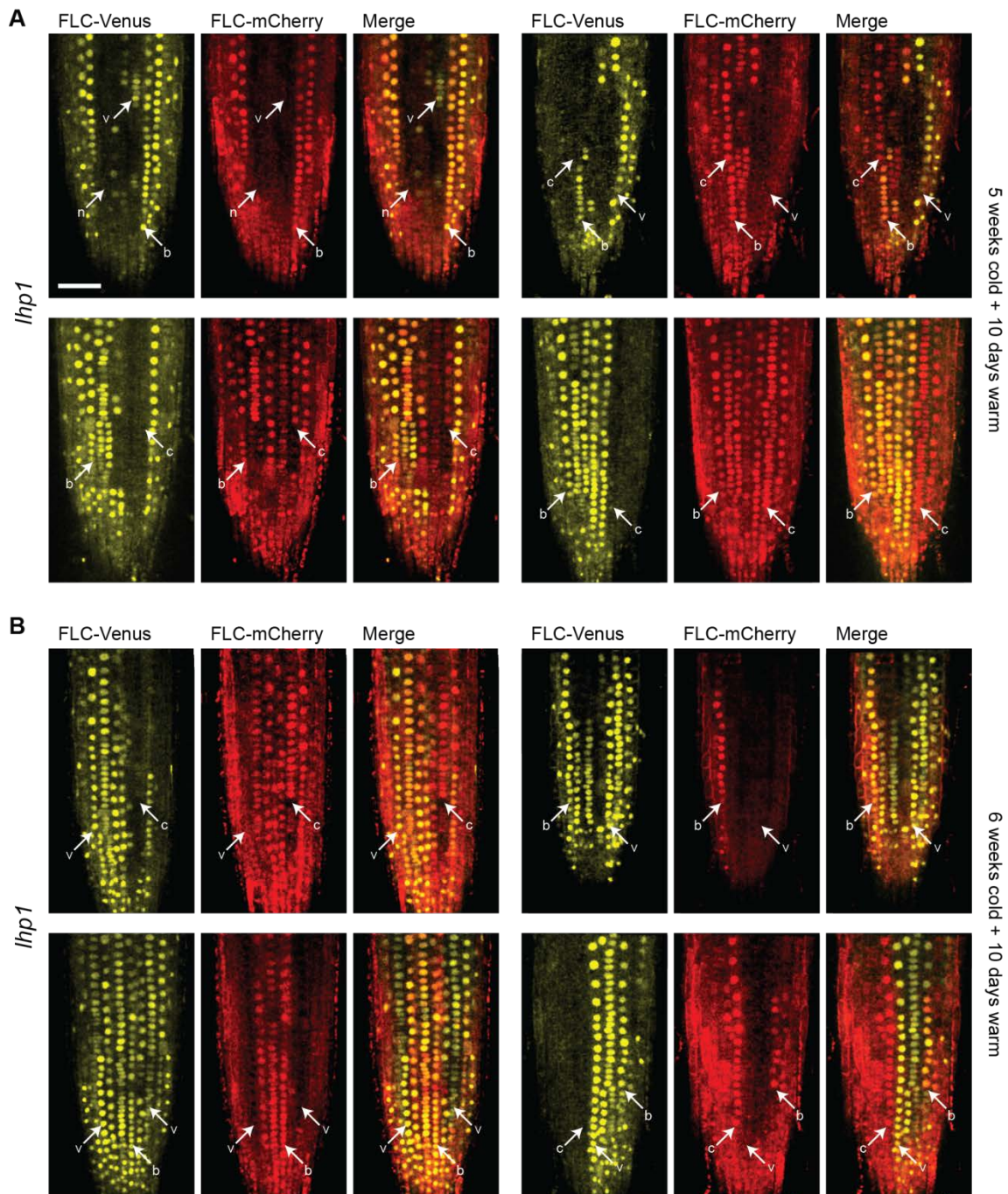
Fig. S9. Imaging FLC-Venus and FLC-mCherry in root meristems in *lhp1* after cold. (A,B)
Imaging FLC-Venus / FLC-mCherry in *lhp1* plants after 5 weeks (A) or 6 weeks (B) cold exposure.
Plants were grown for a further 10 days after cold before imaging. The following notation is used to
label cell files in the various expression states: both expressed, b; FLC-Venus only, v; FLC-mCherry
only, c; neither expressed, n. All plants contain a single genomic copy of each of *FLC-Venus* and
FLC-mCherry. The same image acquisition and processing settings were used for all roots. Both
channels are sum projections over 9 z-slices (8.55 μm). Scale bar shown in (A) is 50 μm, and is valid
for all panels.

396

397
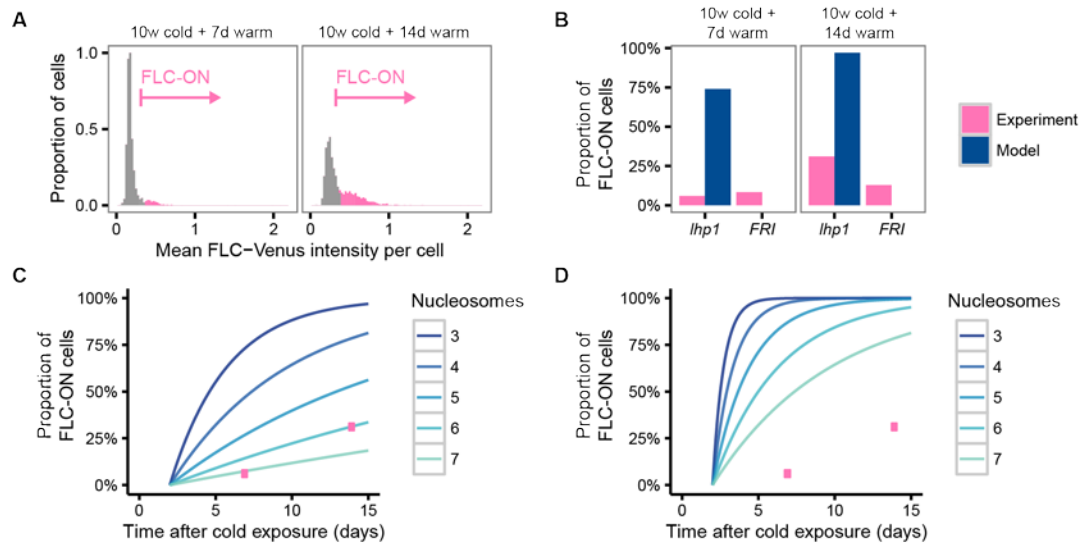
Fig. S10. Comparison of histone-modification-based epigenetic model and experimental data.
(**A**) Histograms of single-cell FLC-Venus intensities in *lhp1*, 7- and 14-days after a 10-week cold treatment. Number of roots and cells analysed for each treatment listed in Table S2. Background levels were estimated as the 98-th percentile of mean cellular FLC-Venus intensity in roots with completely silenced FLC-Venus. Cells below this threshold are shaded grey, while those above (FLC-ON) are shaded pink. (**B**) The proportion of FLC-ON cells measured in wild-type and *lhp1* root meristems after a 10-week cold treatment (Experiment). This is compared to conservative predictions from a model of purely histone-modification-based epigenetic memory in the nucleation region (Model). (**C**) Predicted FLC reactivation dynamics after cold for a histone-modification-based memory model with 3-7 nucleosomes, assuming that a single H3K27me3-containing nucleosome is sufficient for inheritance of silencing. Pink circles show experimental data for *lhp1*, as in (B). (**D**) Same as (C), except with the assumption that two or more H3K27me3-containing nucleosomes must be inherited for silencing.

411

412
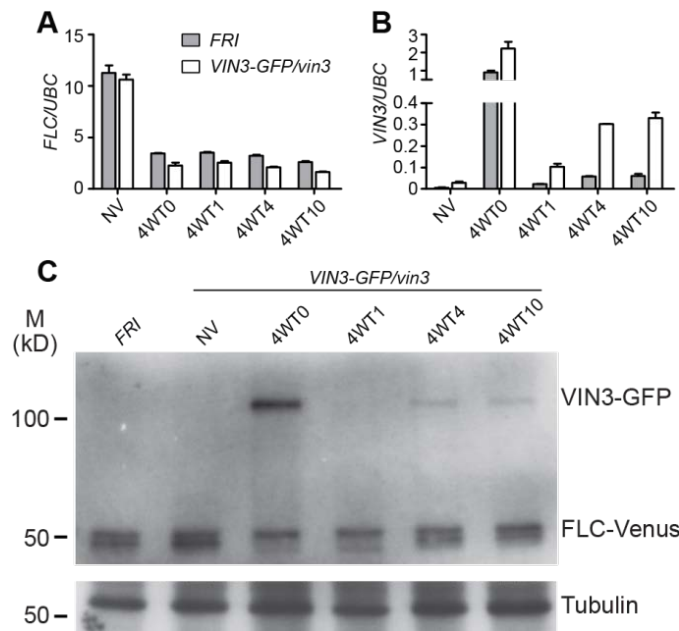
Fig. S11. Characterization of *VIN3-GFP* transgenic line. (A) *FLC* expression in wild-type and
VIN3-GFP/*vin3* plants measured by RT-qPCR before (non-vernalized, NV) and after a 4-week cold
treatment, showing that the *VIN3-GFP* translational fusion complements the *vin3* mutant *FLC*
expression defect during vernalization. **(B)** *VIN3-GFP* transgene mRNA measured by RT-qPCR,
showing that transgene expression in *VIN3-GFP*/*vin3* plants is similar to the endogenous *VIN3* in
wild-type plants during vernalization. Data are represented relative to *UBC*. Note discontinuity in y-
axis. Error bars represent s.e.m from 3 biological replicates in (A) and (B). **(C)** VIN3-GFP was
detected after immunoprecipitation by immunoblot. *FRI* was used as the non-transgene control; FLC-
Venus as the IP efficiency control; and Tubulin as the loading control. Protein size marker is shown in
kDa on the left.

423

424
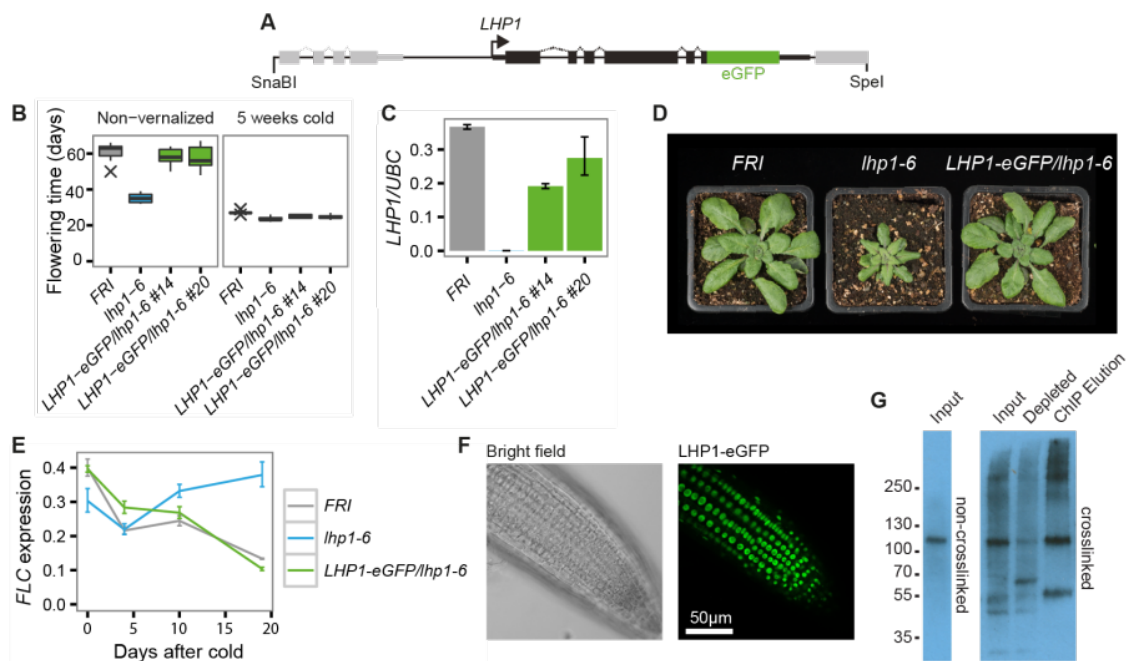
Fig. S12. Characterization of *LHP1-eGFP* transgenic line. (**A**) Schematic of *LHP1-eGFP* construct. Genomic DNA used to generate *LHP1-eGFP* translational fusion is indicated. Exons are represented by black boxes. Transgenes extend from 2.4 kb upstream of ATG to 1.1 kb downstream of the *LHP1* stop codon. Neighbouring genes are depicted in grey. (**B**) The *LHP-eGFP* transgene complements *lhp1-6* flowering time defect in non-vernalized (NV) plants, and transgenic plants respond to a 5-week cold-exposure by accelerating flowering, similar to wild-type. Flowering time was measured by days from sowing until bolting but does not include the time in cold treatment. (**C**) *LHP1* expression measured by RT-qPCR in non-vernalized conditions in wild-type, *lhp1-6* and *LHP1-eGFP/lhp1-6* plants. Transgenic *LHP1-eGFP* restores *LHP1* mRNA expression in *lhp1-6* mutant. Data are represented relative to *UBC*. Error bars represent s.e.m from 3 biological replicates. Two independent *LHP1-eGFP/lhp1-6* transgenic lines are shown. (**D**) Photograph showing that *lhp1-6* plant size and leaf morphology phenotypes are rescued by *LHP1-eGFP* transgene (line #14). (**E**) *FLC* expression measured by RT-qPCR after a 4-week cold treatment in wild-type, *lhp1-6* and *LHP1-eGFP/lhp1-6* plants. *LHP1-eGFP* rescues the *FLC* reactivation phenotype of *lhp1-6*. Data were normalized to *UBC* levels, and are expressed relative to *FLC* levels in non-vernalised plants. *LHP1-eGFP/lhp1-6* represents an average over 3 independent transgenic lines, each measured in 3 biological replicates. Error bars represent s.e.m (n=3 for *FRI*, *lhp1-6*; n=9 for *LHP1-eGFP/lhp1-6*). (**F**) Confocal images showing nuclear localisation of LHP1-eGFP in root meristematic tissue. (**G**) LHP1-eGFP (line #20) can be enriched during ChIP protocol. "non-crosslinked" input sample demonstrates that a single band is present in the absence of crosslinking. Protein size marker is shown in kDa on the left.

445
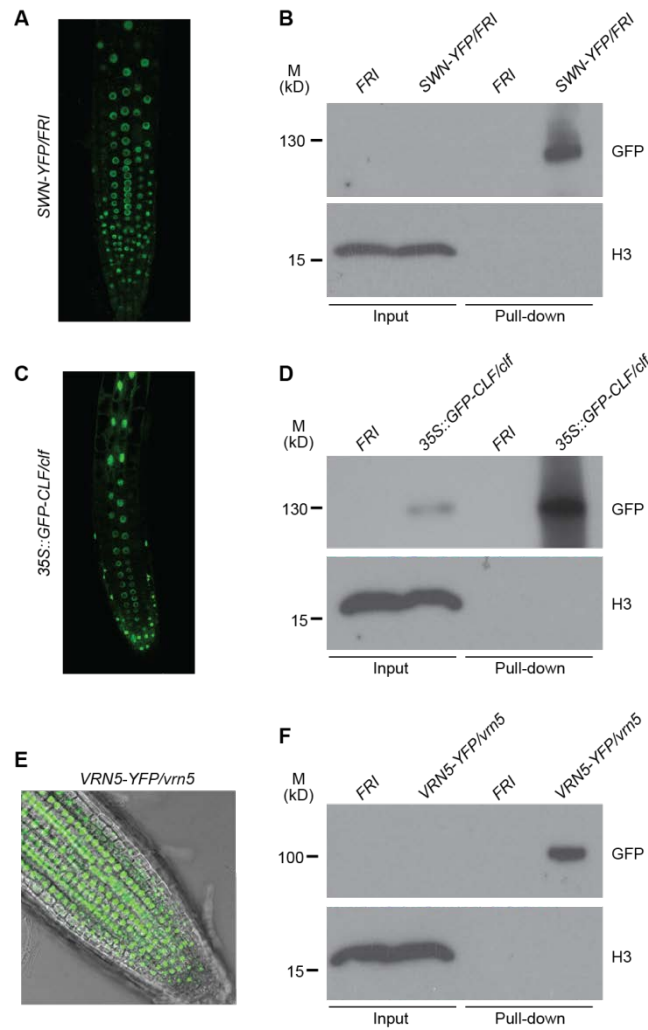
Fig. S13. Detecting SWN, CLF and VRN5 in transgenic lines. Confocal microscope images of root
meristems from **(A)** *SWN-YFP/FRI*, **(C)** *35S::GFP-CLF/clf* and **(E)** *VRN5-YFP/vrn5* plants, showing
nuclear localisation of the GFP fusion proteins. Roots from 9-day old transgenic seedlings were used
for imaging. Corresponding anti-GFP immunoblots **(B, D, F)** from these plants showing that GFP-
tagged proteins are enriched after pull-down. Protein size marker is shown in kDa on the left.
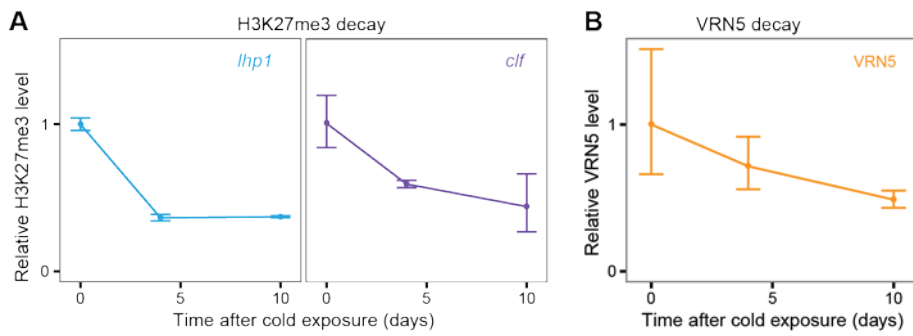
451

452
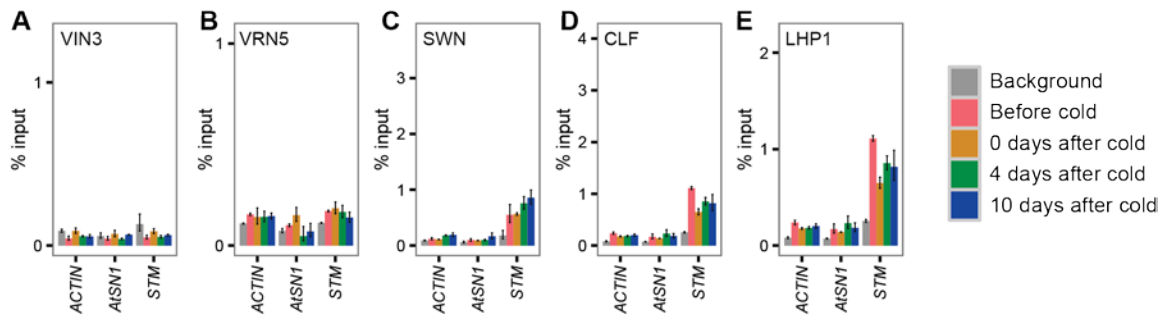
Fig. S14. ChIP for tagged proteins on control genes. (**A**) VIN3, (**B**) VRN5, (**C**) SWN, (**D**) CLF, and (**E**) LHP1 ChIP, before cold and after 6-weeks cold. *FRI* non-vernalized (NV) (background) was used as a non-transgenic control. Error bars represent s.e.m. (n = 3). Scales for y-axis are chosen to be the same as in the corresponding panel in Fig. 4.

457

458

459   **Fig. S15. Comparing H3K27me3 and VRN5 level decay rates at *FLC* nucleation region after a 6-**

460   **week cold treatment.** (**A**) H3K27me3 ChIP data in *lhp1* and *clf* presented as H3K27me3/H3

461   normalised to internal control gene *STM*, averaged over 2 primers for the *FLC* nucleation region, and

462   then further normalized to the end-of-cold level (set as 1). (**B**) VRN5 ChIP enrichment at *FLC*,

463   measured as a percentage of input chromatin, averaged over 2 primers for the *FLC* nucleation region

464   (Table S1), and then normalized to the end-of-cold level (set as 1). Error bars represent s.d. (n = 3 for

465   each primer) in all cases.

466

467
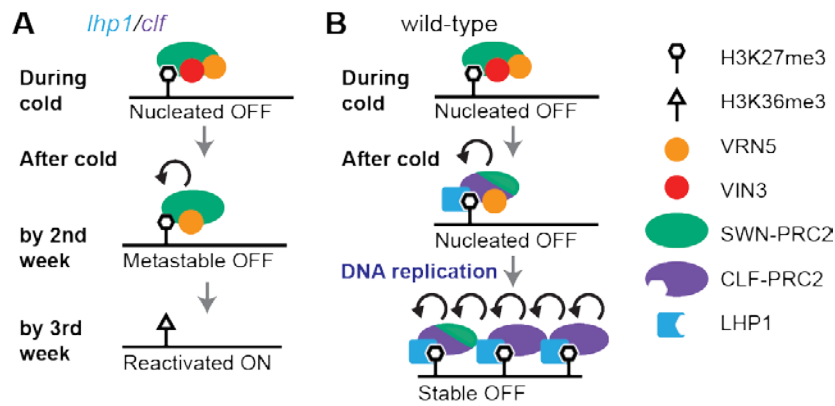
Fig. S16. Schematic model showing the molecular composition of the *FLC* locus during and after cold exposure. (**A**) In *lhp1* and *clf* backgrounds, metastable epigenetic repression is maintained in cis, likely through multiple feedbacks involving VRN5, SWN-PRC2, H3K27me3, and other factors. (**B**) If LHP1 and CLF are present, nucleation can spread to cover the entire locus to achieve fully stable silencing by the feedbacks involving the spread LHP1, CLF-PRC2 and H3K27me3. Circular arrows indicate feedbacks between H3K27me3 and local protein factors. Hybrid green/purple ovals indicate that both CLF-PRC2 and SWN-PRC2 are present.

475

476

477 **Table S1. PCR primers.**

478

Primers used for *FLC* ChIP		
Primer position	Sequence 5'-3'	Note
FLC_-2320_F	ATCCAGAAAAGGGCAAGGAG	
FLC_2267_R	CGAATCGATTGGGTGAATG	
FLC_-1599_F	TGGAGGGAACAACCTAATGC	
FLC_-1530_R	TCATTGGACCAAACCAAACC	
FLC_-392_F	ACTATGTAGGCACGACTTTGGTAAC	
FLC_272_R	TGCAGAAAGAACCTCCACTCTAC	
FLC_-49_F	GCCCGACGAAGAAAAGTAG	
FLC_53_R	TCCTCAGGTTTGGGTTCAAG	
FLC_157_F	CGACAAGTCACCTTCTCCAAA	Nucleation region
FLC_314_R	AGGGGGAACAAATGAAAACC	
FLC_416_F	GGCGGATCTCTTGTTGTTTC	Nucleation region
FLC_502_R	CTTCTTCACGACATTGTTCTTCC	
FLC_652_F	CGTGCTCGATGTTGTTGAGT	
FLC_809_R	TCCCGTAAGTGCATTGCATA	
FLC_1144_F	CCTTTTGCTGTACATAAACTGGTC	
FLC_1257_R	CCAAACTTCTTGATCCTTTTTACC	
FLC_1533_F	TTGACAATCCACAACCTCAATC	
FLC_1670_R	TCAATTTCCTAGAGGCACCAA	
FLC_1933_F	AGCCTTTTAGAACGTGGAACC	Gene Body
FLC_2171_R	TCTTCCATAGAAGGAAGCGACT	
FLC_2465_F	AGTTTGGCTTCCTCATACTTATGG	Gene Body
FLC_2560_R	CAATGAACCTTGAGGACAAGG	
FLC_3197_F	GGGGCTGCGTTTACATTTTA	Gene Body
FLC_3333_R	GTGATAGCGCTGGCTTTGAT	
FLC_3998_F	CTTTTTCATGGGCAGGATCA	Gene Body
FLC_4178_R	TGACATTTGATCCCACAAGC	
FLC_4322_F	AGAACAACCGTGCTGCTTTT	Gene Body
FLC_4469_R	TGTGTGCAAGCTCGTTAAGC	
FLC_5139_F	CCGGTTGTTGGACATAACTAGG	Gene Body
FLC_5244_R	CCAAACCCAGACTTAACCAGAC	
FLC_5643_F	TGGTTGTTATTTGGTGGTGTG	
FLC_5758_R	ATCTCCATCTCAGCTTCTGCTC	
FLC_6057_F	CGTGTGAGAATTGCATCGAG	
FLC_6175_R	AAAAACGCGCAGAGAGAGAG	
FLC_6877_F	TTGTAAAGTCCGATGGAGACG	
FLC_6947_R	ACTCGGCGAGAAAGTTTGTG	
Reference gene for H3K36me3 ChIP		

ACTIN_728_F	GATATTCAGCCACTTGTCTGTG	Reference gene for H3K36me3 ChIP
ACTIN_812_R	CTTACACATGTACAACAAAGAAGG	and for protein ChIP control.
Reference gene for H3K27me3 ChIP		
STM_exon1_F	GCCCATCATGACATCACATC	Reference gene for H3K27me3 ChIP
STM_exon1_R	GGGAACTACTTTGTTGGTGGTG	and for protein ChIP control.
Negative control in protein ChIP		
AtSN1_F	CCAGAAATTCATCTTCTTTGGAAAAG	Protein ChIP control
AtSN1_R	GCCCAGTGGTAAATCTCTCAGATAGA	
Primers for qRT-PCR		
FLC_F	AGCCAAGAAGACCGAACTCA	*FLC* expression
FLC_R	TTTGTCCAGCAGGTGACATC	
VIN3_F	TGCTTGTGGATCGTCTTGTCA	*VIN3* expression
VIN3_R	TTCTCCAGCATCCGAGCAAG	
SWN_F	AGAAATTGCTGGGTTAGTTGTG	*SWN* expression
SWN_R	GAGCATCGAGGACGTACTGAT	
CLF_F	GTAGAAACTGCTGGGTCATTGGT	*CLF* expression
CLF_R	CAGATATTCCAAGTAAAACCCTTTG	
VRN2_F	CAAAGCGCAAAAGAAAGTC	*VRN2* expression
VRN2_R	CAAGAACAATCCTCCCTAACT	
LHP1_F	TGAGGAGTTGGACATCACGA	*LHP1* expression
LHP1_R	CTTCCCATCAGACCTCAGCG	
UBC_qPCR_F	CTGCGACTCAGGGAATCTTCTAA	Reference gene for gene expression
UBC_qPCR_R	TTGTGCCATTGAATTGAACCC	
Primers for genotyping *FLC-Venus* and *FLC-mCherry* transgenes		
FLC-V33-1F	ACAGAGGATCGAGTGGTTT	Use with FLC-V33-2R
FLC-V33-2R	ACATCAGACGAAAGAGAGGA	Use with FLC-V33-1F or pSLJ_RB3
FLC-mC11_1F	ACGCTATGTAAACGTGATTAAGT	Use with FLC-mC11-1R
FLC-mC11_1R	ACCTCAAGATCCGATACATCC	Use with FLC-V33-1F or pSLJ_RB3
pSLJ_RB3	TATTCGGGCCTAACTTTTGGTGTG	T-DNA right border primer

479

480

481   **Table S2. Summary statistics for quantitative image analysis.**

Number of roots imaged				
	FRI	*vin3*	*vrn2*	*lhp1*
NV	8	8	8	8
6WT7	12	13	12	12
7WT7	18	13	13	18
7WT14	21			24
8WT7	16	11	11	19
10WT7	16			16
10WT14	16			17
Number of cells quantified				
	FRI	*vin3*	*vrn2*	*lhp1*
NV	891	885	996	932
6WT7	1807	1662	1515	1804
7WT7	2830	1964	2065	2769
7WT14	3035			2084
8WT7	2276	1550	1486	2357
10WT7	1778			1956
10WT14	1869			1934

482

483